

# UniSymNet: A Unified Symbolic Network Guided by Transformer

Xinxin Li<sup>a</sup>, Juan Zhang<sup>b,c,\*\*</sup>, Da Li<sup>d,e</sup>, Xingyu Liu<sup>b</sup>, Jin Xu<sup>c,d</sup> and Junping Yin<sup>c,d,\*</sup>

<sup>a</sup>School of Mathematical Sciences, East China Normal University, Shang Hai, 200241, China

<sup>b</sup>Institute of Artificial Intelligence, Beihang University, 100191, Beijing, China

<sup>c</sup>Shanghai Zhangjiang Institute of Mathematics, 201203, Shanghai, China

<sup>d</sup>Institute of Applied Physics and Computational Mathematics, 100094, Beijing, China

<sup>e</sup>Academy for Advanced Interdisciplinary Studies, Northeast Normal University, 130024, Changchun, Jilin, China

## ARTICLE INFO

**Keywords:**

Symbolic regression

Transformer model

Symbolic network

## ABSTRACT

Symbolic Regression (SR) is a powerful technique for automatically discovering mathematical expressions from input data. Mainstream SR algorithms search for the optimal symbolic tree in a vast function space, but the increasing complexity of the tree structure limits their performance. Inspired by neural networks, symbolic networks have emerged as a promising new paradigm. However, most existing symbolic networks still face certain challenges: binary nonlinear operators  $\{\times, \div\}$  cannot be naturally extended to multivariate operators, and training with fixed architecture often leads to higher complexity and overfitting. In this work, we propose a **Unified Symbolic Network** that unifies nonlinear binary operators into nested unary operators and define the conditions under which UniSymNet can reduce complexity. Moreover, we pre-train a Transformer model with a novel label encoding method to guide structural selection, and adopt objective-specific optimization strategies to learn the parameters of the symbolic network. UniSymNet shows high fitting accuracy, excellent symbolic solution rate, and relatively low expression complexity, achieving competitive performance on low-dimensional Standard Benchmarks and high-dimensional SRBench.

## 1. Introduction

In the natural sciences, the pursuit of interpretable and simplified models constitutes a fundamental objective. For example, Kepler’s laws of planetary motion, derived from astronomical observations, provided a precise mathematical description of planetary orbits, paving the way for Newton’s theory of gravitation.

Symbolic Regression aligns with this objective by discovering mathematical expressions that capture the underlying relationships in the data. Given a dataset  $\{(x_i, y_i)\}_{i=1}^N$ , the aim is to identify a function  $f(x)$  such that  $y_i \approx f(x_i)$  for all  $i$ . SR has proven effective in various fields, from the derivation of physical laws based on empirical data (Udrescu and Tegmark, 2020) to the advancement of research in materials science (Wang et al., 2019). However, unlike traditional regression, SR requires discovering both functional forms and parameters without prior structural assumptions, which makes SR challenging. SR generally involves two stages: (i) searching the functional structure space for viable functional skeletons, then (ii) optimizing parameters for the selected structure. How to represent the functional structure space remains a challenge due to the diversity and complexity of real physical equations.

Most research in SR uses symbolic trees to construct the functional structure space. Specifically, the symbolic tree representation method encodes basic operators and variables

as tree nodes and represents equations in the form of a pre-order traversal for the forward pass process. As a result, SR tasks are transformed into the problem of searching for the optimal symbolic tree within a vast symbolic tree space. To tackle this, Genetic Programming (GP)-based methods (Schmidt and Lipson, 2009) employ biology-inspired strategies to conduct this search, while Reinforcement Learning (RL)-based methods (Petersen et al., 2020; Tenachi et al., 2023) leverage risk-seeking policy gradients to guide the search process. These methods learning from scratch contrast with Transformer-based methods (Biggio et al., 2021; Kamienny et al., 2022), which adapt the machine translation paradigm from NLP (Vaswani, 2017; Devlin et al., 2019) to symbolic tree search (Valipour et al.). Their pre-training mechanisms allow them to improve with experience and data.

Recently, based on the theoretical foundation of the Universal Approximation Theorem (Hornik et al., 1989), deep neural networks demonstrate remarkable capabilities to approximate complex functions and capture intricate nonlinear patterns within high-dimensional data spaces. In this context, EQL (Martius and Lampert, 2017) introduced modifications to feed-forward networks by incorporating interpretable components, such as replacing standard activation functions with operators like  $\cos$  and  $\sin$ , thus transforming them into symbolic networks. Since then, an increasing number of SR methods based on symbolic network representations have emerged (Sahoo et al., 2018; Liu et al., 2023; Li et al.), demonstrating competitive performance against methods based on symbolic tree representations. Moreover, compared to the black-box nature of standard neural networks, symbolic networks are transparent and possess better extrapolation capabilities, which has led to their increasing

\*Corresponding author

\*\*Principal corresponding author

✉ 51265500102@stu.ecnu.edu.cn (X. Li); zhang\_juan@buaa.edu.cn (J. Zhang); dli@enu.edu.cn (D. Li); ZY2342118@buaa.edu.cn (X. Liu);

xujin22@gscaep.ac.cn (J. Xu); yinjp829829@126.com (J. Yin)

ORCID(s): 0009-0008-8962-0084 (X. Li)

use in scientific exploration and discovery (Long et al., 2019; Kim et al., 2020).

In symbolic network,  $\{+, -\}$  and scalar multiplication operator are implemented through affine transformations, while  $\{\times, \div, \text{pow}\}$  are implemented using activation functions. This method has two advantages: 1) it allows  $\{+, -\}$  to extend from binary operators in symbolic trees to multivariate operators, and 2) the symbolic network can support cross-layer connections through the id operator (Wu et al., 2023). These features help reduce the length of the equation representation. However, as noted in current research (Martius and Lampert, 2017; Sahoo et al., 2018; Li et al.), pow operators are typically restricted to activation functions with predefined real exponents (e.g., squaring  $(\cdot)^2$  or taking the square root  $\sqrt{\cdot}$ ), which inherently limits the expressive power of network.

Integrating operators  $\{\times, \div, \text{pow}\}$  into neural architectures as naturally as  $\{+, -\}$  and scalar multiplication operators would align more closely with human intuition. In algebra, the isomorphism between the multiplicative group  $(\mathbb{R}^+, \times)$  and the additive group  $(\mathbb{R}, +)$  is established through the homomorphic mapping  $\ln$  and its inverse  $\exp$  (Lang, 2012), which provides a unified framework for translating nonlinear operators into linear ones. This transformation has been successfully applied in machine learning to enhance numerical stability and computational efficiency, such as log softmax (Goodfellow et al., 2016) and logarithmic likelihood of probability calculation. Inspired by the above, we propose using nested unary operators  $\{\ln, \exp\}$  to represent binary operators  $\{\times, \div, \text{pow}\}$ , thus establishing a **Unified Symbolic Network** consisting solely of Unary operators (UniSymNet). In the UniSymNet,  $\{\times, \div\}$  are transformed from binary operators in symbolic trees into multivariate operators, similar to  $\{+, -\}$ .

UniSymNet not only implements the above changes in its network representation but also introduces a more flexible and learning-from-experience framework. Specifically, EQL uses backpropagation within a fixed neural network framework, tending to cause overfitting and generate overly complex expressions, which contradicts the fundamental goal of natural science research. In this study, we pre-train a Transformer model to guide structural selection, and adopt objective-specific optimization strategies to learn the parameters of the symbolic network.

In summary, we introduce the main contributions of this work as follows:

- We introduce UniSymNet, a symbolic network that unifies binary operators  $\{\times, \div, \text{pow}\}$  into nested unary operators  $\{\ln, \exp\}$ , and define the conditions under which UniSymNet can reduce depth and node count.
- We propose a novel label encoding method that ensures a pre-trained Transformer model guides the structure discovery of UniSymNet.
- We demonstrate that UniSymNet outperforms several representative baseline methods across in-domain and

out-of-domain settings, covering low-dimensional Standard Benchmarks and high-dimensional SRBench.

The remainder of this paper is organized as follows: Section 2 reviews recent works in SR. Section 3 details the framework of UniSymNet, including its core mechanisms and implementation. Sections 4 and 5 describe the experimental setup and present detailed results, respectively. Section 6 discusses the specific differences between UniSymNet and conventional symbolic tree representations. Section 7 summarizes key findings and contributions, while Section 8 outlines future research directions to extend this methods.

## 2. Related Works

### 2.1. Genetic Programming for Symbolic Regression

Traditional Symbolic Regression (SR) methods were predominantly based on Genetic algorithm (Forrest, 1993), in particular, genetic programming (GP) (Koza, 1994). GP-based methods iteratively evolve symbolic trees through selection, crossover, and mutation, optimizing their fit to observed data. Subsequent advancements, such as the development of Eureqa (Dubčáková, 2011), improved the scalability and efficiency of GP-based SR. However, these methods (La Cava et al., 2018; Virgolin et al., 2021) still face challenges, including high computational costs, sensitivity to hyperparameters, and difficulties in scaling well to large datasets or high-dimensional problems.

### 2.2. Neural Networks for Symbolic Regression

In more recent studies, neural networks have been integrated with Symbolic Regression (SR) tasks, primarily to enhance the search for mathematical expressions. For example, AIFeynman (Udrescu and Tegmark, 2020) used fully connected neural networks to identify simplified properties of underlying function forms (e.g., multiplicative separability), effectively narrowing down the search space by decomposing complex problems into smaller subproblems. Similarly, DSR (Petersen et al., 2020) utilized a recurrent neural network (RNN) to generate symbolic trees, refining its expression generation based on a reward signal that adjusts the likelihood of generating better-fitting expressions.  $\Phi$ -SO (Tenachi et al., 2023) extends this method by embedding unit constraints to incorporate physical information into the symbolic framework.

Unlike prior methods that employ neural networks to accelerate symbolic search, recent methods explore neural network as novel frameworks for constructing interpretable symbolic representations. EQL (Martius and Lampert, 2017) transformed fully connected networks into symbolic networks by using operators such as  $\sin$ ,  $\cos$ ,  $\times$  as activation functions, but it didn't introduce  $\div$  operator. Therefore, in EQL<sup>+</sup> (Sahoo et al., 2018), the nonlinear binary operators  $\{\times, \div\}$  are incorporated into the network through the architectural design illustrated in Fig. 1. In such symbolic networks, the  $l$ -th layer contains  $p_l$  unary operators and  $q_l$  binary operators, where  $q_l = d_l - p_l$  and  $d_l$  denotes the total number of operators in this layer. Since each unary

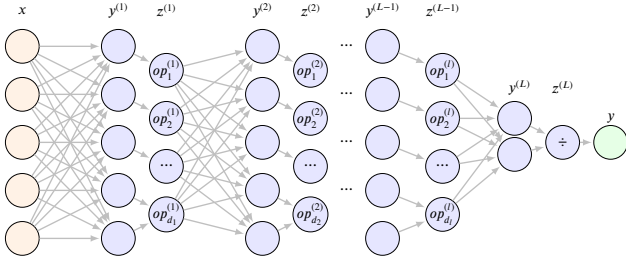


Figure 1: The overall architecture of EQL<sup>‡</sup>.

operator consumes one input node whereas each binary operator requires two input nodes, the preceding layer must provide  $n_l = p_l + 2q_l$  input nodes to satisfy the computational requirements of this layer. This input configuration, denoted as  $y^{(l)}$ , therefore contains  $n_l$  nodes prior to operator application. Following the application of operators, the resulting vector  $z^{(l)}$  contains  $d_l$  nodes, the forward propagation rules are defined as follows:

$$\begin{aligned}
 z^{(0)} &= x, \quad x \in \mathbb{R}^{d_0}, \\
 y^{(l)} &= W^{(l)} z^{(l-1)} + b^{(l)}, \quad l = 1, 2, \dots, L, \\
 z_i^{(l)} &= \text{op}_i^{(l)}(y_i^{(l)}), \quad i = 1, 2, \dots, p_l, \\
 z_i^{(l)} &= \text{op}_{i+p_l}^{(l)}(y_{p_l+2i-1}^{(l)}, y_{p_l+2i}^{(l)}), \quad i = 1, 2, \dots, q_l,
 \end{aligned} \tag{1}$$

where  $z^{(l-1)} \in \mathbb{R}^{d_{l-1}}$  is the previous layer’s output,  $W^{(l)} \in \mathbb{R}^{n_l \times d_{l-1}}$ ,  $b^{(l)} \in \mathbb{R}^{n_l}$  are the weight matrix and bias vector for the current layer, respectively. In this way, EQL<sup>‡</sup> not only has strong fitting and expressive capabilities but also offers better interpretability compared to black-box models. However, the operator pow is typically constrained to fixed exponents when used as activation functions, limiting its flexibility in modeling arbitrary polynomial relationships. These methods use backpropagation within a fixed neural network framework, so they face challenges related to overfitting and the generation of highly complex results. Meanwhile, DySymNet (Li et al.) employed an RNN controller to sample various symbolic network architectures guided by policy gradients, demonstrating effectiveness in solving high-dimensional problems. These methods typically perform symbolic regression from scratch and, as a result, do not improve with experience.

In addition, recent studies have proposed novel representation methods: ParFam(Scholl et al.) incorporates residual neural networks with rational function layers to parameterize mathematical expressions; GraphDSR (Liu et al., 2025) models mathematical expressions as directed acyclic graphs (DAGs) and optimizes symbolic constants through graph neural networks (GNNs).

### 2.3. Transformer Model for Symbolic Regression

The Transformer model, introduced by (Vaswani, 2017), represents a pivotal advancement in deep learning. Its remarkable success has driven its extensive adoption across various domains, including SR tasks. NeSymReS(Biggio

et al., 2021) was the first to use a large-scale pre-trained Transformer model to discover symbolic trees from input-output pairs, improving performance with more data and computational resources, but it is limited to low-dimensional problems. SymbolicGPT (Valipour et al.) converted the point cloud of the dataset into order-invariant vector embeddings and used a GPT model to translate them into mathematical expressions in string form that describe the point sets. Kamienny et al. (2022) proposed an end-to-end symbolic regression method using a Transformer model to predict complete mathematical expressions, including constants, boosting inference speed while maintaining high accuracy. TPSR(Shojaee et al., 2023) combined pre-trained Transformer models with Monte Carlo Tree Search to optimize program sequence generation by considering non-differentiable performance feedback.

## 3. Methods

Given a dataset  $\{(x_i, y_i) \in \mathbb{R}^d \times \mathbb{R}\}_{i=1}^N$ , SR seeks to identify a mathematical function  $f$  that approximates the relationship  $y_i \approx f(x_i)$  for all observations. This process inherently involves a dual optimization challenge: (1) exploring the space of potential functional skeletons, and (2) determining optimal parameters for each candidate structure. Formally, we frame symbolic regression as a bi-level optimization problem:

$$s^*, \theta^* = \arg \min_{s \in \mathcal{S}} \left( \min_{c \in \mathcal{C}_s} \sum_{i=1}^N (y_i - f_s(x_i; c))^2 \right), \tag{2}$$

where  $\mathcal{S}$  represents the space of functional skeletons (each defining a function  $f_s(x; c)$ ), and  $\mathcal{C}_s$  denotes the parameter space for structure  $s$ . The inner optimization identifies the optimal parameters  $\theta$  for a given skeleton, while the outer optimization selects the best-performing skeleton configuration.

Our method solves the bi-level optimization problem, consisting of outer optimization for structural discovery and inner optimization for parameter estimation. Figure 2 illustrates the overall architecture. For the outer optimization problem, our method has three key components: Structural Space Formalization, Structure-to-Sequence Encoding, and UniSymNet Structure Inference. For the inner optimization problem, we implement objective-specific optimization strategies: Differentiable Network Optimization and Symbolic Function Optimization. As for how to select based on the objective, we will provide a detailed discussion in Section 5.1.3.

### 3.1. Structural Space Formalization

Fig. 3 illustrates the architectural configuration  $\mathcal{A}$  of UniSymNet, which comprises two main components: the depth  $L$  and the assignment of layer-specific operators. Specifically, the network depth is defined as the number of hidden layers, while the assignment of layer-specific operators is specified such that the  $l$ -th layer consists of  $d_l$

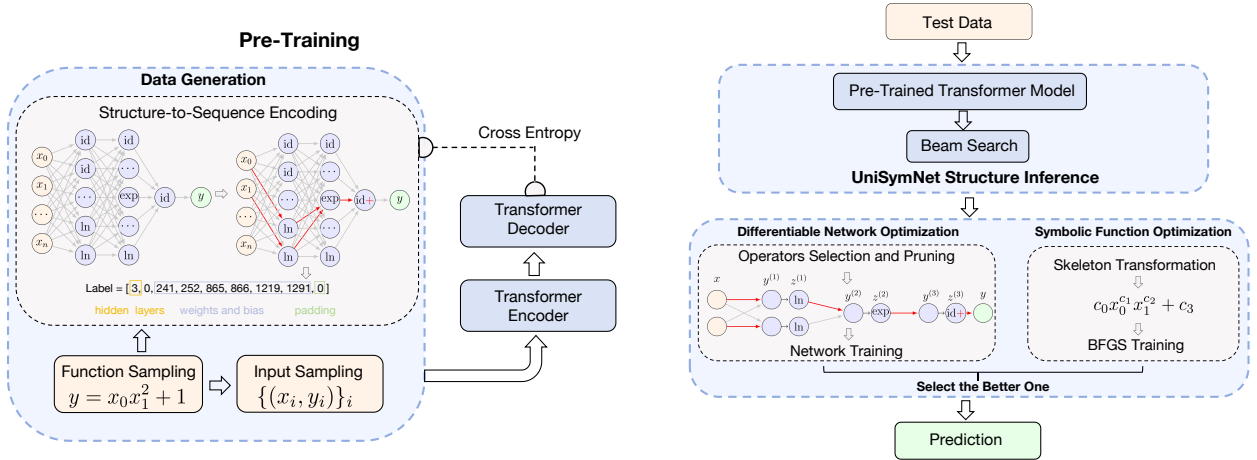


Figure 2: The overall architecture of our method.

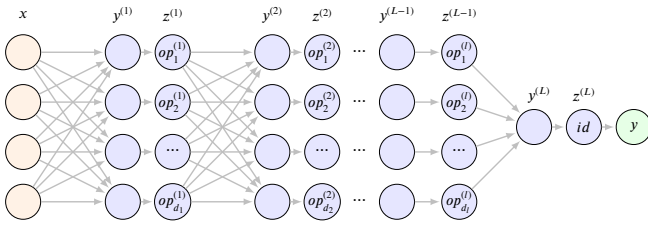


Figure 3: The overall architecture of UniSymNet.

nodes and is associated with the set of operators  $\{op_i^{(l)}\}_{i=1}^{d_l}$ . The operators are selected from a unary operator library  $\mathcal{O}_u = \{id, \sin, \cos, \exp, \ln\}$ .

With the architecture  $\mathcal{A}$ , it is natural to inquire about the forward propagation process of the network. For a fully-connected neural network, the forward propagation is governed by the following principles:

$$\begin{aligned} z^{(0)} &= x, \quad x \in \mathbb{R}^{d_0}, \\ y^{(l)} &= W^{(l)} z^{(l-1)} + b^{(l)}, \quad l = 1, 2, \dots, L, \\ z_i^{(l)} &= op_i^{(l)}(y_i^{(l)}), \quad i = 1, 2, \dots, d_l, \end{aligned} \quad (3)$$

where  $z^{(l-1)} \in \mathbb{R}^{d_{l-1}}$  is the previous layer's output,  $W^{(l)} \in \mathbb{R}^{d_l \times d_{l-1}}$ ,  $b^{(l)} \in \mathbb{R}^{d_l}$  are the weight matrix and bias vector for the current layer, respectively.

To effectively represent the functional skeleton of a symbolic network structure, we convert a fully-connected neural network into a sparsely-connected one by employing a collection of binary mask matrices,  $\mathcal{M} = \{M_w^{(l)}, M_b^{(l)}\}_{l=1}^L$ . In other words, during forward propagation, the following modifications are applied:

$$W^{(l)} = W^{(l)} \odot M_w^{(l)}, \quad b^{(l)} = b^{(l)} \odot M_b^{(l)}, \quad l = 1, \dots, L, \quad (4)$$

where  $M_w^{(l)}$  has the same dimensions as the weight matrix  $W^{(l)}$  for the  $l$ -th layer, and  $M_b^{(l)}$  has the same dimensions as the bias vector  $b^{(l)}$ .

Now that all operators are selected from  $\mathcal{O}_u$ , a natural question arises regarding the treatment of binary operators  $\mathcal{O}_b = \{+, -, \times, \div, \text{pow}\}$ . Evidently, the linear binary operators  $\mathcal{O}_b^{lin} = \{+, -\}$  are integrated into the affine transformations described in Equation 3. As introduced in Section 1, we establish unified symbolic representations  $\Psi$  for nonlinear binary operators  $\mathcal{O}_b^{non-lin} = \{\times, \div, \text{pow}\}$  through nested compositions of unary operators  $\{\ln, \exp\}$ ,

$$\begin{aligned} \Psi(x_1 \times x_2) &\triangleq \exp(\ln x_1 + \ln x_2) \\ \Psi(x_1 \div x_2) &\triangleq \exp(\ln x_1 - \ln x_2) \\ \Psi(\text{pow}(x, \lambda)) &\triangleq \exp(\lambda \cdot \ln x), \quad \lambda \in \mathbb{R} \end{aligned} \quad (5)$$

This operator unification can be systematically expressed as:

$$\Psi(\mathcal{O}_b^{non-lin}) \triangleq \mathcal{O}_u^{\otimes n} \circ \mathcal{O}_b^{lin}, \quad (6)$$

where  $\mathcal{O}_u^{\otimes n}$  indicates nested compositions of unary operators  $\{\ln, \exp\}$ ,  $\circ$  represents the interaction between two operations. It should be noted that  $\Psi^{-1}$  refers to the inverse transformation, which recovers the original nonlinear operators by reversing the nesting of unary operators.

The impact of the  $\Psi$  transformation on network complexity highlights its advantages. In Theorem 1 and Theorem 2, we show that, under specific conditions, applying the mapping  $\Psi$  can reduce both the depth and the number of nodes in a symbolic network, thereby lowering its overall complexity. For simplicity, we call the symbolic network with the  $\Psi$  transformation as UniSymNet, and the symbolic network without the  $\Psi$  transformation as EQL-type Network. The proof of theorems will be given in the Appendix A.

**Theorem 1.** Let  $P(\mathbf{x}) = \sum_{k=1}^K c_k \prod_{i=1}^d x_i^{m_{ki}}$ , where  $c_k \in \mathbb{R}$ ,  $m_{ki} \in \mathbb{R} \setminus \{0\}$  and  $d, k \in \mathbb{N}$ . Suppose that  $\exists(k_0, i_0)$ , s.t.  $m_{k_0 i_0} \neq 1$ . Then, for any function  $P(\mathbf{x})$ , there exists a UniSymNet architecture that can represent it exactly using depth  $L_1$  and  $N_1$  nodes. Likewise, it can also be represented by an EQL-type network with depth  $L_2$  and  $N_2$  nodes.

For  $d \geq 2$ , it holds that  $L_1 \leq L_2$  and  $N_1 \leq N_2$ . That means, for any such function  $P(\mathbf{x})$  with  $d \geq 2$ , the UniSymNet architecture achieves representational efficiency that is better than or equal to that of EQL-type networks in terms of both depth and node count.

It is worth noting that functions in the form of  $P(\mathbf{x})$  are often used in the PDE Discover (Long et al., 2019) task. Furthermore, we present the corollary of Theorem 1.

**Theorem 2.** *Under the hypotheses of Theorem 1, consider replacing each  $x_i$  with  $g_i(\mathbf{x})$ . Suppose each  $g_i(\mathbf{x})$  is represented by a UniSymNet with depth  $L_{1i}$  and node count  $N_{1i}$  and a EQL-type with depth  $L_{2i}$  and node count  $N_{2i}$ . If  $\max\{L_{1i}\} \leq \max\{L_{2i}\}$  and  $\sum_i N_{1i} \leq \sum_i N_{2i}$ , then for  $P(g_1(\mathbf{x}), \dots, g_d(\mathbf{x}))$ , the conclusion of Theorem 1 still hold.*

For tasks targeting the learning of high-dimensional functional relationships of the form  $P(\cdot)$ , UniSymNet should be preferentially selected due to its superior representational efficiency in both architectural depth and node complexity.

To represent a functional skeleton  $f_s$  and then establish the structural space, the network architecture  $\mathcal{A}$  alone is not sufficient. Therefore, we define the structure of UniSymNet as  $S = (\mathcal{A}, \mathcal{M})$ , where the structural space  $S$  encompasses all valid combinations of architectural configurations and mask matrices, formally represented as the Cartesian product  $S = \mathcal{A} \times \mathcal{M}$ . To establish a direct connection between the structure  $S$  and its functional skeleton  $f_s$  (e.g.,  $c_0 x_0^{c_1} x_1^{c_2}$ ), we introduce a systematic mapping  $\Phi(S) : S \rightarrow f_s$  formalized by the Equation 7:

$$\begin{aligned} z^{(0)} &= [x_0, x_1 \dots, x_{d_0}]^\top, \\ y^{(l)} &= \left( C_w^{(l)} \odot M_w^{(l)} \right) z^{(l-1)} + \left( C_b^{(l)} \odot M_b^{(l)} \right), \quad l = 1, \dots, L, \\ z^{(l)} &= \left[ \text{op}_1^{(l)}(y_1^{(l)}), \dots, \text{op}_{d_l}^{(l)}(y_{d_l}^{(l)}) \right]^\top, \\ f_s &= \Psi^{-1}(z^{(L)}), \end{aligned} \quad (7)$$

where  $C_w^{(l)}$  and  $C_b^{(l)}$  denote symbolic matrices, whose shapes align with the binary masks  $M_w^{(l)}$  and  $M_b^{(l)}$ . The Hadamard product  $\odot$  ensures that symbolic constants  $C_i^{(l)}$  are assigned only to positions marked by 1s in the mask matrices. During computation, constants fulfilling equivalent roles are merged to simplify expressions. For example,  $c_0(c_1 x_0 + c_2)$  collapses to  $c_0 x_0 + c_1$ , where redundant constants are absorbed.

### 3.2. Structure-to-Sequence Encoding

In Section 3.1, we define the structure of UniSymNet as  $S = (\mathcal{A}, \mathcal{M})$ . To encode  $S$  into a sequence compatible with transformer-based frameworks, we face a key challenge: the variable shapes of  $\mathcal{M}$  across different architectures  $\mathcal{A}$  make it difficult to construct a unified embedding of  $\mathcal{A}$  and  $\mathcal{M}$ . To address this issue, we partially constrain  $\mathcal{A}$  and sampling sub-networks via sparsified  $\mathcal{M}$ , masking redundant components. Specifically, we adopt the following strategies:

- (i) Each layer is populated with a predefined sequence of unary operators from the set  $\mathcal{O}_u$ . Specifically, The operators are arranged in the fixed order of  $\mathcal{O}_u$ . Each operator is replicated  $m$  times per layer, resulting in  $5m$  units per layer. For example, with  $m = 2$ , a layer contains  $2 \times \text{id}$ ,  $2 \times \sin$ ,  $2 \times \cos$ ,  $2 \times \exp$ , and  $2 \times \ln$ .
- (ii) The width (i.e., number of nodes per layer) is uniformly set to  $5m$  for all layers. The depth  $L$  is limited to a maximum value  $L_{\max}$ , allowing flexibility in depth while ensuring computational tractability.
- (iii) The sparse mask matrix set  $\mathcal{M}$ , governed by the forward propagation rules in Equation 7, prunes redundant connections while preserving the predefined operator sequence and width.

Therefore, the labels consist of three components: the depth  $L$ ,  $\{M_w^{(l)}\}_{l=1}^L$  and  $\{M_b^{(l)}\}_{l=1}^L$ . The number of hidden layers is designated as the first component of the label, followed by a separator 0 as the second component. Subsequently, all matrices in  $\mathcal{M}$  are flattened and concatenated to form a unified vector. The label  $\mathcal{L}$  corresponding to the structure  $S$  can be expressed as:

$$\begin{aligned} E &= [L, 0, M_w^{(1)}(1, 1), M_w^{(1)}(1, 2), \dots, M_w^{(1)}(5m, d), \dots, \\ &M_w^{(l)}(i, j), \dots, M_w^{(L)}(1, 1), \dots, M_w^{(L)}(1, 5m), \\ &M_b^{(1)}(1), \dots, M_b^{(1)}(5m), \dots, M_b^{(l)}(i), \dots, M_b^{(L)}(1)]. \end{aligned}$$

where  $M_w^{(l)}(i, j)$  denotes the element at position  $(i, j)$  in the mask matrix of the  $l$ -th layer. It is important to note that, since the width of the  $L$ -th layer is 1, both  $M_w^{(L)}$  and  $M_b^{(L)}$  have only one row. To effectively shorten the length of the label while retaining the essential structural information of UniSymNet, we implement a transformation defined by the following operation:

$$\begin{aligned} \mathcal{I} &= \{i \mid i \geq 3, E_i = 1\} = \{i_1, i_2, \dots, i_{|\mathcal{I}|}\}, \\ \mathcal{E} &= [L, 0, i_1 - 2, i_2 - 2, \dots, i_{|\mathcal{I}|} - 2]. \end{aligned} \quad (8)$$

where  $\mathcal{I}$  represents the indices of all elements starting from the third position ( $i \geq 3$ ) where the value equals 1,  $i - 2$  applies an index offset adjustment to each qualifying index. Thus, the transformation of the structure  $S$  into a sequence  $\mathcal{E}$  is completed.

### 3.3. UniSymNet Structure Inference

To implement the outer optimization in Equation 2, we use a parameterized set-to-sequence model  $M_\theta$  that maps a collection of input-output pairs  $\mathcal{D} = \{(x_i, y_i)\}_{i=1}^N$  to the symbolic sequence  $\mathcal{E}$  defining the structure  $S$  of UniSymNet. The model architecture adopts an encoder-decoder framework: the encoder projects the dataset  $\mathcal{D}$  into a latent space through permutation-invariant operations, producing a fixed-dimensional representation  $z$  that encapsulates the input-output relational features; subsequently, the decoder autoregressively generates the target sequence  $\mathcal{E}$  by computing conditional probability distributions  $\mathcal{P}(\mathcal{E}_{k+1} | \mathcal{E}_{1:k}, z)$

at each step, where the next token prediction is conditioned on both the latent code  $z$  and the preceding token sequence  $\mathcal{E}_{1:k}$ . We first pre-train the model on large synthetic datasets of varied math expressions to improve generalization, then adapt it to specific SR tasks. The left panel of Fig. 2 describes the process of pre-training  $M_\theta$ , which mainly includes data generation and training.

### 3.3.1. Data Generation

Each training instance consists of two components: a set of data points  $\mathcal{D}$ , which serves as the input, and the sequence  $\mathcal{E}$ , serving as the label. The data generation follows three main steps, with the parameters involved in the data generation process provided in Appendix B.

**Function Sampling:** We follow the method proposed by Lample and Charton (2019) to sample functions  $f$  and generate random trees with mathematical operators as internal nodes and variables or constants as leaves. The process is as follows:

- (i) **Constructing the Binary Tree:** The input dimension  $d$  is drawn from a uniform distribution  $\mathcal{U}\{1, d_{\max}\}$ , and the number of binary operators  $b_{\text{op}}$  is sampled from  $\mathcal{U}\{d-1, b_{\max}\}$ . The  $b_{\text{op}}$  binary operators are then selected from the operator library  $\mathcal{O}_b$ .
- (ii) **Inserting Unary Operators:** The number of unary operators  $u_{\text{op}}$  is sampled from  $\mathcal{U}\{0, u_{\max}\}$ , and  $u_{\text{op}}$  unary operators are chosen randomly from  $\mathcal{O}_u$  and inserted into the tree.
- (iii) **Applying Affine Transformations:** Affine transformations are applied to selected variables  $\{x_j\}$  and unary operators  $\{u_j\}$ . Each variable  $x_j$  is transformed to  $wx_j + b$ , and each unary operator  $u_j$  becomes  $wu_j + b$ , where the parameters  $(w, b)$  are sampled from the distribution  $\mathcal{D}_{\text{aff}}$ . This step mimics the linear transformations in UniSymNet.

Then, we get the function  $f$ . The first  $d$  variables are sampled in ascending order to ensure the correct input dimensionality. This method avoids the appearance of functions with missing variables, such as  $x_1 + x_3$ .

**Input Sampling:** We independently sample  $\{x_i\}_{i=1}^N \subset \mathbb{R}^d$  in an  $d$ -dimensional space. The  $j$ -th element  $x_{i,j}$  in  $x_i$  follows a uniform distribution  $\mathcal{U}(S_{1,j}, S_{2,j})$ , with  $S_{1,j}$  and  $S_{2,j}$  defining the range of the  $j$ -th dimension. We impose the constraint that  $S_{1,j}, S_{2,j} \in (-10, 10)$  for all  $j$ , ensuring the sampling remains within a specified range. The corresponding output values  $\{y_i\}_{i=1}^N$  are computed by  $y_i = f(x_i)$ . During this process, each  $x_i$  is padded with zeros to match a fixed feature dimension  $d_{\max}$ . If any  $y_i$  contains NaN values, the corresponding pair  $(x_i, y_i)$  is replaced entirely with zeros. It’s worth noting that the dataset  $\{(x_i, y_i)\}_{i=1}^N$  is converted from floating-point values to a multi-hot bit representation to mitigate potential numerical instability due to large variations in  $y$ , following the IEEE-754 standard.

**Label Encoding:** For a random function  $f$ , the initial step is to identify the structure  $S$  of the UniSymNet associated with

the functional skeleton  $f_s$ , detailed in Appendix F. Then, we convert  $S$  to the label sequence  $\mathcal{E}$  as described in Section 3.2. As a final step, the label sequences are padded to a uniform length with a padding token. We still face the challenge that the same function can be represented in different forms, resulting in different labels for the same function, such as  $x_0 + \sin(2x_1)$  and  $x_0 + 2 \sin(x_1) \cos(x_1)$ . Therefore, we merge different labels of equivalent expressions by assigning the label of the shorter sequence.

### 3.3.2. Training

After generating the training dataset, we begin training the Transformer model  $M_\theta$ . The full training procedure is detailed in Algorithm 1.

---

#### Algorithm 1 Transformer Model Training

---

- 1: **Input:** Transformer model  $M_\theta$ , batch size  $B$ , training distribution  $\mathcal{P}_{\mathcal{E}, \mathcal{D}}$ , learning rate  $\eta$ , maximum iterations  $K$ , similarity tolerance  $\epsilon$
  - 2: Initialize  $\mathcal{L}_{\text{prev}} \leftarrow \infty$
  - 3: **for**  $k = 1$  to  $K$  **do**
  - 4:    $\mathcal{L}_{\text{train}} \leftarrow 0$
  - 5:   **for**  $i = 1$  to  $B$  **do**
  - 6:      $e, (X, Y) \leftarrow \text{sample from } \mathcal{P}_{\mathcal{E}, (X, Y)}$
  - 7:      $\mathcal{L}_{\text{train}} \leftarrow \mathcal{L}_{\text{train}} - \sum_k \log P_{M_\theta}(e_{k+1} | e_{1:k}, \mathcal{D})$
  - 8:   **end for**
  - 9:   Update  $\theta$  using  $\theta \leftarrow \theta - \eta \nabla_\theta \mathcal{L}_{\text{train}}$
  - 10:   Compute  $\mathcal{L}_{\text{val}}$  on the validation set
  - 11:   **if**  $0 < \mathcal{L}_{\text{prev}} - \mathcal{L}_{\text{val}} < \epsilon$  **then**
  - 12:     **break**
  - 13:   **end if**
  - 14:   Update  $\mathcal{L}_{\text{prev}} \leftarrow \mathcal{L}_{\text{val}}$
  - 15: **end for**
- 

Once the model  $M_\theta$  has been trained, given a test dataset  $\mathcal{D}$ , we perform beam search (Goodfellow et al., 2016) to obtain a set of candidate sequences  $\mathcal{E}$ .

## 3.4. Symbolic Function Optimization

For each candidate sequence  $\mathcal{E}$ , we transform the structure  $S$  of UniSymNet into functional skeletons  $f_s$  according to Equation 7. It’s worth noting that UniSymNet merges nested exp and ln operators into a nonlinear binary operator during skeleton transformation, which helps avoid numerical instability. We then randomly assign specific exponent values in the skeleton to commonly encountered values in natural systems, such as  $\mathcal{V} = \{1, -1, 0.5, -0.5, 2, -2, 3, -3\}$ . However, directly enumerating all combinations leads to an exponential increase in the search space complexity, which results in a significant computational cost. To address this, we maintain a learnable probability distribution  $P_\theta(v_i | \mathcal{V})$  for each exponent position  $v_i$  in the equation, representing the priority of assigning different exponent values.

To enable differentiable discrete sampling, we adopt the Gumbel-Softmax trick:

$$v_i = \text{Gumbel-Softmax} \left( \frac{\log P_\theta(v_i) + g_i}{\tau} \right), \quad (9)$$

where  $g_i \sim \text{Gumbel}(0, 1)$  is a noise term used to perturb the logits, and  $\tau(t) = \tau_0 \exp(-kt/T)$  is a temperature parameter that controls the degree of approximation to one-hot sampling. The key challenge is how to guide the sampling of exponents and optimize the parameters effectively. To this end, we adopt the risk-seeking policy gradient method proposed by Petersen et al. (2020). For each sampled symbolic skeleton  $f_s(x; c)$ , we optimize the constants  $c^*$  using the BFGS(Nocedal and Wright, 1999) method to minimize the mean squared error (MSE):

$$c^* = \arg \min_c \sum_{i=1}^N (f_s(x_i; c) - y_i)^2.$$

Based on the optimized results, we define a reward function:

$$R = 1/(1 + \text{MSE}),$$

which ensures that higher-performing candidates receive higher rewards.

To focus the optimization on promising candidates, we calculate the  $1-\epsilon$  quantile of the reward distribution, denoted by  $R_\epsilon(\theta)$ , and compute the policy gradient only for samples with rewards above this threshold:

$$\nabla_\theta J_{\text{risk}} \propto \mathbb{E}_{R \geq R_\epsilon(\theta)} [R \nabla_\theta \log P_\theta(f_s)] + \lambda_{\mathcal{H}} \nabla_\theta \mathcal{H}(P_\theta),$$

where  $\mathcal{H}(P_\theta)$  denotes the entropy of the policy distribution, and the coefficient  $\lambda_{\mathcal{H}}$  controls the level of exploration. This entropy term prevents premature convergence to suboptimal solutions.

### 3.5. Differentiable Network Optimization

For each candidate sequence  $\mathcal{E}$ , we generate a corresponding set of mask matrices  $\mathcal{M}$ . These matrices serve two critical roles in optimizing the UniSymNet. First, they enable structural simplification by eliminating unconnected neural nodes, thereby reducing the unified architecture  $\mathcal{A}$  (introduced in Section 3.2) to a lightweight variant  $\mathcal{A}'$ . Second, the matrices act as dynamic pruning masks that sparsify inter-node connectivity during forward propagation, accelerating convergence and reducing the complexity of derived symbolic expressions. As illustrated in Fig. 4 for the case  $c_0 x_0^{c_1} x_1^{c_2}$ , this process simplifies the network topology while preserving functional equivalence.

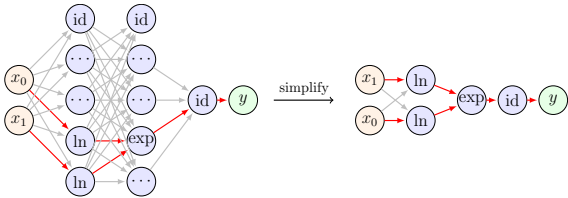


Figure 4: The process of simplifying UniSymNet’s structure.

With the structure  $\mathcal{S}$ , the UniSymNet is trained via standard backpropagation with a stabilized loss function

combining prediction error and activation regularization:

$$\mathcal{L} = \underbrace{\left| \min(0, x - \theta_{\text{ln}}) \right| + \max(0, |x| - \theta_{\text{exp}})}_{\text{Activation Regularization } \mathcal{L}_{\text{penalty}}} + \frac{1}{N} \sum_{i=1}^N (\hat{y}_i - y_i)^2,$$

where the regularized activation functions are defined as:

$$\text{ln}_{\text{reg}}(x) = \begin{cases} 0 & x < \theta_{\text{ln}}, \\ \ln(|x| + \epsilon) & \text{otherwise,} \end{cases}$$

$$\text{exp}_{\text{reg}}(x) = \begin{cases} \exp(\theta_{\text{exp}}) & x \geq \theta_{\text{exp}}, \\ \exp(x) & \text{otherwise.} \end{cases}$$

And the  $\theta_{\text{ln}}$  and  $\theta_{\text{exp}}$  are activation thresholds that suppress unstable regions of logarithmic and exponential operators respectively, with  $\epsilon > 0$  ensuring numerical safety.

In Section 3.1, we introduced a pruning strategy that can be applied during the forward propagation process according to Equation 4. Since the pruning strategy may affect the gradient backpropagation during network training, potentially impacting the model’s accuracy, its application during training is optional. The specific criteria for selecting whether to apply pruning during training will be discussed in detail in Section 5.1.2.

## 4. Experiments

### 4.1. Metrics

In scientific discovery contexts,  $f$  is further required to be simplified and interpretable, capturing governing laws underlying the data. Thus, the goal of symbolic regression is not only to achieve high fitting accuracy but also to ensure low complexity and high symbolic solution rate(La Cava et al., 2021).

We evaluate **fitting performance** using  $R^2$ , a higher  $R^2$  indicates a higher fitting accuracy of the model, defined as follows:

**Definition 1.** For  $N_{\text{test}}$  independent test samples, the coefficient of determination  $R^2$  is defined as:

$$R^2 = 1 - \frac{\sum_{i=1}^{N_{\text{test}}} (y_i - \hat{y}_i)^2}{\sum_{i=1}^{N_{\text{test}}} (y_i - \bar{y})^2},$$

where  $N_{\text{test}}$  is the number of test samples,  $y_i$  is the true value of the  $i$ -th sample,  $\hat{y}_i$  is the predicted value of the  $i$ -th sample, and  $\bar{y}$  is the mean of the true values.

We assess the **complexity** using the Def. 2 and calculate the complexity of the models after simplifying via sympy(Meurer et al., 2017).

**Definition 2.** A model’s complexity is defined as the number of mathematical operators, features, and constants in the model, where the mathematical operators are drawn from a set  $\{+, -, \times, \div, \sin, \cos, \exp, \ln, \text{pow}, \text{abs}\}$ .

For the ground-truth problems, we use the **Symbolic Solution** defined as Def. 3 to capture models that differ from the true model by a constant or scalar.

**Definition 3.** A model  $\hat{\phi}(x, \hat{\theta})$  is a Symbolic Solution to a problem with ground-truth model  $y = \phi^*(x, \theta^*) + \epsilon$ , if  $\hat{\phi}$  does not reduce to a constant, and if either of the following conditions are true: 1)  $\phi^* - \hat{\phi} = a$ ; or 2)  $\phi^*/\hat{\phi} = b, b \neq 0$ , for some constants  $a$  and  $b$ .

Extrapolation ability reflects whether a model can effectively generalize to unseen domains in practice. It is well known that conventional neural networks, such as black-box models (e.g., MLPs), are often limited in their **extrapolation ability**. Similarly, we are interested in evaluating the extrapolation ability of symbolic networks. If a model satisfies the definition of a symbolic solution (Def. 3), it indicates strong extrapolation ability. However, for models that do not meet this definition, we evaluate their extrapolation ability using the following criterion.

**Definition 4.** Let  $D_{\text{train}} = \{(X, y)\}$  be a training set with inputs  $X$  sampled from an interval  $[a, b] \subset \mathcal{X}$ , where  $\mathcal{X}$  denotes the domain of  $X$ . The corresponding test set is constructed with inputs sampled from the extended interval  $[a-c, b+c] \cap \mathcal{X}$ . The extrapolation ability is evaluated using the  $R^2$  score computed on this test set.

## 4.2. Datasets

To comprehensively evaluate our model and compare its performance with the baselines, we conduct tests on various publicly available datasets, with the detailed information provided in Appendix C. We categorize the datasets into two groups based on their dimension.

**Standard Benchmarks:** The feature dimension of the datasets in the Standard Benchmarks satisfies  $d \leq 2$ . The Standard Benchmarks consist of eight widely used public datasets: Koza(Koza, 1994), Keijzer(Keijzer, 2003), Nguyen(Uy et al., 2011), Nguyen\*(Nguyen with constants), R rationals(Krawiec and Pawlak, 2013), Jin(Jin et al., 2019), Livermore(Mundhenk et al., 2021), Constant.

**SRBench:** The feature dimension of most datasets in SRBench(La Cava et al., 2021) satisfies  $d \geq 2$ . SRBench used black-box regression problems available in PMLB(Olson et al., 2017) and extended PMLB by including 130 datasets with ground-truth model forms. These 130 datasets are sourced from the Feynman Symbolic Regression Database and the ODE-Strogatz repository, derived from first-principles models of physical systems.

## 4.3. Baselines

In our experiments, we evaluate the performance of our method against several baselines, which can be categorized into two main types: In-domain methods and Out-of-domain methods. The comprehensive overview of baselines is provided in Appendix G.

We compare the performance of our method against In-domain SR methods, including the *transformer-based*

*methods* SymbolicGPT (Valipour et al.), NeSymRes (Biggio et al., 2021), End-to-End (Kamienny et al., 2022) and TPSR (Shojaee et al., 2023), as well as the *symbolic network-based method* EQL (La Cava et al., 2018), *neural guided method* DySymNet (Li et al.) and ParFam (Scholl et al.). The Out-of-domain methods refer to the 14 SR methods mentioned in SRBench(La Cava et al., 2021), with the 14 SR methods primarily consisting of GP-based and DL-based methods.

## 5. Results

### 5.1. Ablation Studies

We performed a series of ablation studies on 200 randomly generated equations, which were not part of the training set, focusing on three key aspects: encoding methods, pruning strategy and parameter optimization.

#### 5.1.1. Ablation Study on Encoding methods

We evaluated the influence of two encoding methods on model performance: *Symbolic Tree method* encoding symbolic trees via prefix traversal(Biggio et al., 2021), and *UniSymNet Structure method* encoding the UniSymNet structure  $S$  as a label in Section 3. To eliminate the influence of the parameter optimization method, both methods use standard BFGS optimization without reinforcement learning to guide the optimization direction.

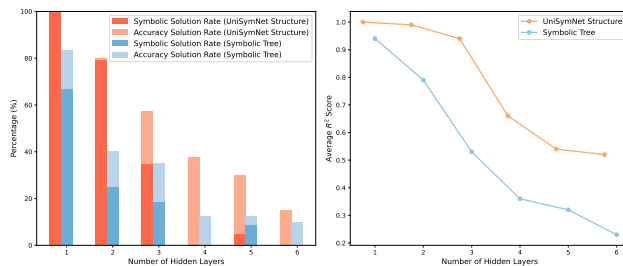


**Figure 5:** Performance comparison of two encoding methods as the number of hidden layers in the equation varies.

In Fig. 5, the x-axis represents the number of hidden layers  $L$  in the UniSymNet corresponding to the equations in the test set. A higher  $L$  value indicates a more complex equation. The left panel shows, for each encoding method, both the accuracy solution rate at  $R^2 > 0.99$  and the symbolic solution rate decline as  $L$  increases. The right panel shows two methods’ performance on the average  $R^2$  score. Both panels reveal that the model’s performance declines as  $L$  increases, due to the decreasing accuracy of the Transformer’s predictions as the target equations become more complex. Nonetheless, the UniSymNet-structure encoding method consistently maintains better performance than another method, demonstrating the superiority of the *UniSymNet Structure method* encoding.

#### 5.1.2. Ablation Study on Pruning Strategy

In Section 3.5, we mentioned that the pruning strategy can be integrated into the training process selectively. To investigate its impact on experimental performance, we designed

three comparison methods. The *Without Guidance method* sets the UniSymNet structure to a default form ( $L = 3, m = 2$ ). The *Only Architecture method* uses a Transformer to guide the architecture  $\mathcal{A}$  of UniSymNet and doesn't add pruning strategy. The *Architecture and Pruning Strategy method* uses a Transformer to guide both the architecture  $\mathcal{A}$  and the mask set  $\mathcal{M}$  and adds pruning strategy.

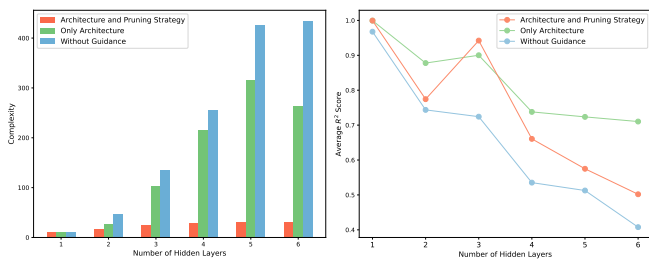


**Figure 6:** Performance comparison of three methods as the number of hidden layers in the equation varies.

In Fig. 6, the left panel compares expression complexity for the three methods as the number of hidden layers  $L$  increases. We observe that introducing the pruning strategy significantly reduces complexity. The right panel shows the *Only Architecture method* achieves the best fitting performance, followed by the *Architecture and Pruning Strategy method*, while the *Without Guidance method* performs the worst. Overall, architectural guidance is effective, while pruning does not improve fitting performance. This phenomenon can be attributed to two factors. First, the structure predicted by the Transformer is not always absolutely accurate. Since guidance is applied only at the architectural level, the network retains the ability to self-adjust and refine its internal structure during training. Second, the application of pruning strategies may interfere with gradient propagation, potentially affecting final performance. However, the pruning strategy significantly reduces expression complexity.

### 5.1.3. Ablation Study on Parameter Optimization

When applying our method, the choice between the *Symbolic Function Optimization method* and the *Differentiable Network Optimization method* depends on the specific objective. As noted in Section 5.1.2, *Differentiable Network Optimization method* itself can be carried out with or without pruning strategy. How to choose between these three methods is what we are going to discuss next.

Because the pruned UniSymNet  $\mathcal{S}$  corresponds exactly to the symbolic function structure  $f_s$ , their complexities coincide. In other words, pruning produces expression complexity similar to that of the Symbolic Function Optimization method, while skipping pruning leads to higher complexity than both alternatives. Therefore, we focus on symbolic accuracy and fitting performance, excluding complexity from comparison. For simplification, we denote the *Symbolic Function Optimization method* as method-1, the *Differentiable Network Optimization method* with pruning strategy as method-2, and the one without pruning strategy as method-3.

**Table 1**

Performance comparison of parameters optimization methods.

| Metrics                | Method-1 | Method-2 | Method-3 |
|------------------------|----------|----------|----------|
| Average $R^2$ Score    | 0.7754   | 0.7421   | 0.8216   |
| Symbolic Solution Rate | 0.3333   | 0.1515   | 0.1224   |

Table 1 shows that method-1 achieves the highest symbolic solution rate, while method-3 demonstrates the best fitting performance. A natural question arises: why does method-2's  $\mathcal{S}$  exhibit a one-to-one correspondence with method-1's  $f_s$ , yet method-1's Symbolic Solution Rate is significantly inferior to method-2's? There are two reasons. On the one hand, the BFGS algorithm is more appropriate for models with relatively few parameters, in contrast to neural networks, which typically involve large-scale parameter optimization. On the other hand, redundant parameters tend to emerge in symbolic networks. For example, equivalent expressions like  $w_1(w_0x_0 + b_0)$  and  $c_0x_0 + c_1$  may coexist despite their mathematical equivalence.

Therefore, each method is suited to distinct objectives:

- (i) If a reliable surrogate model is the primary goal, method-3 serves as an excellent choice.
- (ii) If uncovering underlying relationships or scientific discoveries within the data is desired, method-1 is preferable. This also makes it one of the most suitable methods for symbolic regression tasks.
- (iii) For specialized tasks such as derivative computation, symbolic networks with built-in automatic differentiation offer a clear advantage. In such cases, method-2 provides a lower-complexity surrogate compared to method-3, though with a slight reduction in fitting accuracy.

## 5.2. In-domain performance

The problem sets in the Standard Benchmarks have at most two variables and simple ground-truth equations. We test our method on these benchmarks and compare it against the in-domain baselines.

### 5.2.1. Fitting Performance and Complexity

A model that is too simple may fail to capture the underlying relationships within the data, resulting in poor fitting performance. However, an excessively complex model may fit the data well, but it also risks overfitting and lacks interpretability. Achieving a good balance requires a model with relatively low complexity and high fitting accuracy. Thus, we present a joint comparison of fitting performance and complexity in this section.

As a first step, we compare the fitting performance separately. Fig. 7 presents the fitting performance comparison of in-domain methods on the Standard Benchmarks. To enhance clarity, the rings in Fig. 7 are intentionally spaced unevenly. Based solely on the average  $R^2$  score across each dataset, ParFam, UniSymNet, DySymNet, and TPSR exhibit

**Table 2**

Fitting accuracy ( $R^2 > 0.99$ ) and complexity comparison of in-domain methods.

| Benchmark | Metrics | EQL    | NeSymRes | End-to-End    | DySymNet      | ParFam        | TPSR          | UniSymNet     | Ground-Truth |
|-----------|---------|--------|----------|---------------|---------------|---------------|---------------|---------------|--------------|
| Koza      | Com     | 5.00   | 9.00     | 16.83         | 14.00         | 23.65         | 16.83         | <b>13.00</b>  | 11.00        |
|           | Acc     | 0.0000 | 0.5000   | <b>1.0000</b> | <b>1.0000</b> | <b>1.0000</b> | <b>1.0000</b> | <b>1.0000</b> | -            |
| Keijzer   | Com     | 17.93  | 9.45     | 22.45         | 17.20         | 81.68         | <b>15.64</b>  | 14.25         | 10.83        |
|           | Acc     | 0.4583 | 0.5833   | 0.6708        | 0.8333        | 0.9667        | <b>1.0000</b> | 0.8333        | -            |
| Nguyen    | Com     | 15.85  | 9.08     | 22.75         | 24.20         | 92.30         | <b>14.42</b>  | 15.42         | 9.20         |
|           | Acc     | 0.2958 | 0.4167   | 0.8458        | 0.8333        | <b>1.0000</b> | <b>1.0000</b> | <b>1.0000</b> | -            |
| Nguyen*   | Com     | 17.70  | 8.07     | 16.12         | 16.00         | 39.54         | 15.40         | <b>13.00</b>  | 9.58         |
|           | Acc     | 0.5500 | 0.6000   | <b>1.0000</b> | <b>1.0000</b> | <b>1.0000</b> | <b>1.0000</b> | <b>1.0000</b> | -            |
| R         | Com     | 9.00   | 12.30    | 21.83         | 14.33         | 24.97         | 19.00         | <b>13.67</b>  | 18.67        |
|           | Acc     | 0.3167 | 0.3333   | 0.6667        | 0.6667        | <b>1.0000</b> | 0.6667        | <b>1.0000</b> | -            |
| Jin       | Com     | 17.11  | 8.95     | 28.19         | 120.00        | 107.69        | <b>24.11</b>  | 19.50         | 13.00        |
|           | Acc     | 0.0167 | 0.1667   | 0.9667        | <b>1.0000</b> | <b>1.0000</b> | <b>1.0000</b> | 0.5000        | -            |
| Livermore | Com     | 14.72  | 8.09     | 20.95         | 23.30         | 38.55         | 17.20         | <b>12.27</b>  | 9.73         |
|           | Acc     | 0.2682 | 0.2727   | 0.6614        | 0.9091        | <b>1.0000</b> | 0.9545        | <b>1.0000</b> | -            |
| Constant  | Com     | 21.47  | 7.42     | 16.30         | 23.30         | 29.11         | <b>14.75</b>  | 13.87         | 7.63         |
|           | Acc     | 0.5313 | 0.5000   | <b>1.0000</b> | 0.6250        | <b>1.0000</b> | <b>1.0000</b> | 0.8750        | -            |

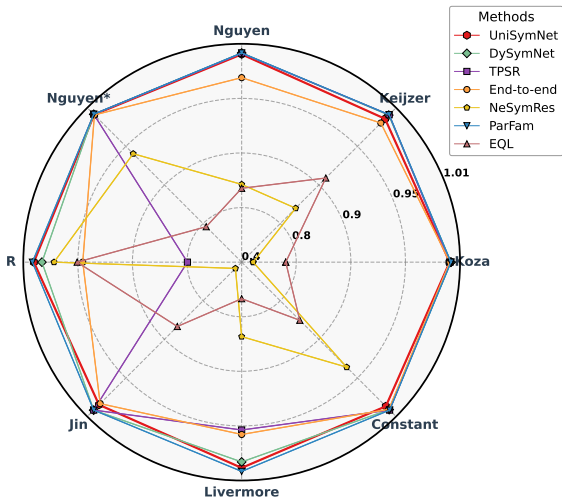


**Figure 7:** Average  $R^2$  score comparison of in-domain methods on Standard Benchmarks.

competitive performance, among which ParFam consistently demonstrates superior fitting capability, while UniSymNet shows the next best performance.

And to enable a more detailed joint comparison, Table 2 provides a comprehensive analysis of each method in terms of fitting accuracy ( $R^2 > 0.99$ ) and expression complexity. The "Ground-truth" column in Table 2 represents the true average complexity for each dataset. We highlight methods that achieve 100% fitting accuracy in bold and mark the one with the lowest complexity among them. As shown, UniSymNet strikes a good balance between fitting accuracy and complexity, achieving perfect fitting accuracy with the lowest complexity on the Koza, Nguyen, R, and Livermore datasets. However, UniSymNet performs less favorably on

the Jin and Constant datasets, primarily because more than half of the equations in these datasets do not satisfy the conditions specified in Section 3.1.

### 5.2.2. Computational Efficiency

We also consider the time cost of solving the problems. Therefore, we compare the average test time of the in-domain methods on the Standard Benchmarks. Fig. 8

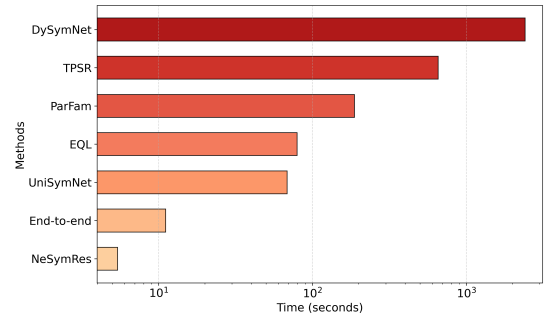


**Figure 8:** Average test time comparison of in-domain methods.

compares the test time of various in-domain methods. The learning-from-experience methods: NeSymRes, End-to-end and UniSymNet achieve the shortest test time, benefiting from the strong guidance provided by pre-trained models, and the other methods generally exhibit longer test time.

### 5.2.3. Extrapolation Ability

To compare the extrapolation capabilities of symbolic networks and standard neural networks, we conducted evaluations on most of the Standard Benchmarks datasets, including Keijzer, Nguyen, Constant, and Livermore. Our comparison included the Transformer-based SR methods NeSymRes and UniSymNet, as well as the machine learning

methods SVR and MLP. The training datasets used in our experiments are the same as in the previous section, while the extrapolation test sets span intervals twice the length of the training ranges. Fig. 9 presents a qualitative comparison on extrapolation ability. UniSymNet outperforms the other methods in interpolation and extrapolation  $R^2$  score, demonstrating superior extrapolation ability.

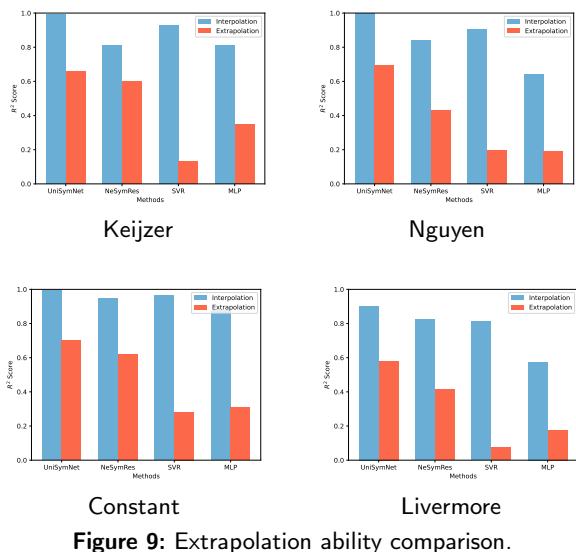


Figure 9: Extrapolation ability comparison.

To provide a more detailed illustration, we conducted an in-depth evaluation of the specific Livermore-13 and Nguyen-1 problems. Fig. 10 presents extrapolation ability comparison on the ground-truth problems Livermore-13 ( $x^2$ ) and Nguyen-1 ( $x^3 + x^2 + x$ ). While all four methods effectively fit the training data, SR methods outperform traditional machine learning methods (MLP and SVR) in the out-of-domain performance. On the Livermore-13 and Nguyen-1 problems, our method closely fits the ground truth, accurately capturing the underlying patterns.

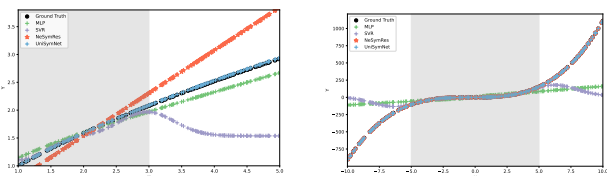


Figure 10: Extrapolation ability comparison on the Livermore-13 and Nguyen-1 problems.

### 5.3. Out-of-domain performance

We evaluated our method using the ground-truth problems in SRBench, including 133 datasets: 119 SR datasets from Feynman, and 14 SR datasets from ODE-Strogatz. Each dataset was provided with different levels of noise: 0, 0.001, 0.01, and 0.1. We compared the performance of different methods across three metrics: symbolic solution rate, fitting performance, and expression complexity.

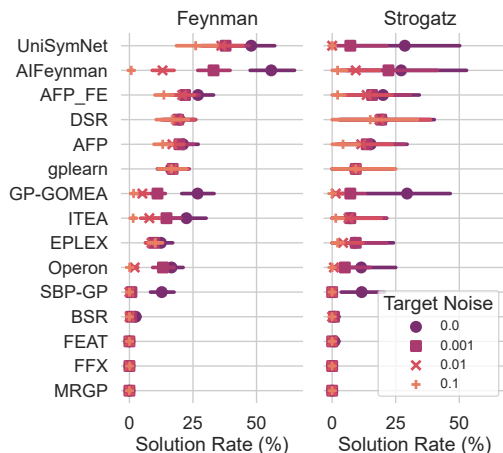


Figure 11: Symbolic solution rate comparison of 14 out-of-domain methods on SRbench under different noise levels.

#### 5.3.1. Symbolic Solution Rate

Fig. 11 shows a comparison of the symbolic solution rate between UniSymNet and 14 out-of-domain methods on the ground-truth problems. The left panel shows that our method performs slightly worse than AI-Feynman on the Feynman datasets only when the noise level is zero. The right panel presents that our method achieves the highest symbolic solution rate on the ODE-Strogatz datasets at zero noise, but the performance degrades more noticeably as the noise level increases. Overall, UniSymNet demonstrates strong capability in recovering true symbolic expressions.

#### 5.3.2. Fitting Performance and Complexity

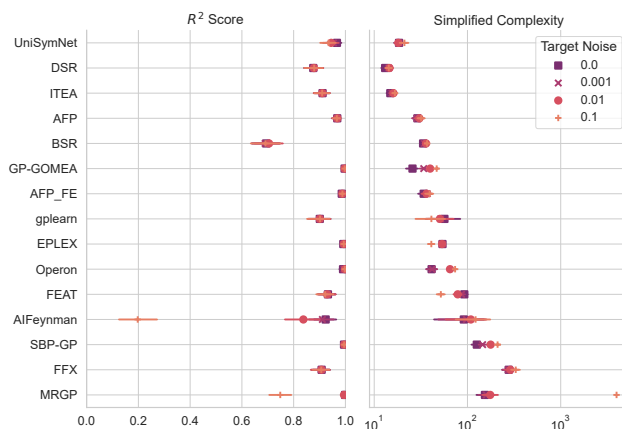
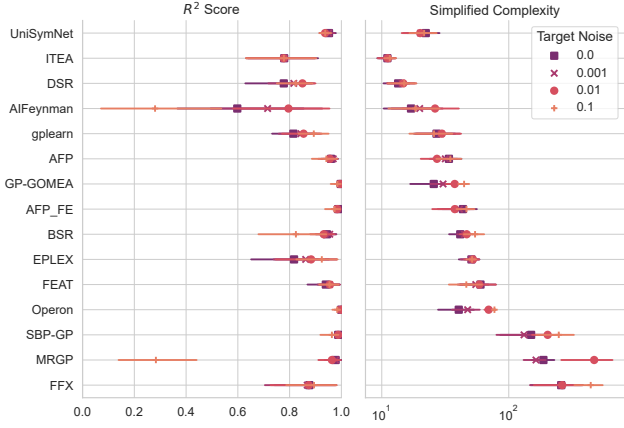


Figure 12: Performance comparison of 14 out-of-domain methods on the Feynman datasets under different noise levels.

Fig. 12 shows fitting performance and complexity comparisons on Feynman datasets. Our method achieves an average  $R^2$  score of **0.9672** on the Feynman datasets, while ranks third in terms of expression complexity. This indicates that, given a similar level of expression complexity, our method provides better fitting performance.



**Figure 13:** Performance comparison of 14 out-of-domain methods on the ODE-Strogatz datasets under different noise levels.

Fig. 13 shows fitting performance and complexity comparisons on ODE-Strogatz datasets. UniSymNet achieved an average  $R^2$  score of **0.9522** on this dataset, while also maintaining a relatively low level of expression complexity.

Overall, UniSymNet shows strong fitting performance and low complexity across both datasets. Fig. 12 and Fig. 13 further show that our method remains stable under varying noise levels, indicating the robustness of our method to different levels of noise.

## 6. Discussion

### 6.1. Symbolic Trees vs. Unified Symbolic Networks

Symbolic trees represent mathematical expressions hierarchically, leaves represent operands (constants/variables), internal nodes denote operators, and edges define operational dependencies. However, unified symbolic networks represent mathematical expressions through forward propagation: input nodes encode variables, hidden layers apply operations, and edges carry learnable weights. Then we will discuss the differences between them.

**Linear Transformation:** Symbolic Networks replace the  $\{+, -\}$  operators with linear transformations, implying that the  $\{+, -\}$  operators are no longer confined to binary operators but can achieve multivariate interactions, thereby adapting to high-dimensional feature spaces. The linear transformations in symbolic networks inherently constitute affine mappings in vector spaces, therefore the expressive capacity of symbolic networks forms a superset encompassing all linear operations achievable by symbolic trees. For the  $i$ -th node in Equation 3, linear transformation can be written as:

$$y_i^{(l)} = \sum_{j=1}^{d_{l-1}} W_{ij}^{(l)} z_j^{(l-1)} + b_i^{(l)}, \quad \forall i = 1, 2, \dots, d_l, \quad (10)$$

However, for the linear transformation in Equation 10, symbolic tree representation requires constructing a binary tree

structure for each  $i$ -th node. Its minimum depth grows as:

$$\text{Depth}_{\text{tree}} = \left\lceil \log_2 \left( \sum_{j=1}^{d_{l-1}} \delta_{ij} \right) \right\rceil + 1,$$

where  $\delta_{ij} \in \{0, 1\}$  indicates whether the connection  $W_{ij}$  exists. For example, Fig. 14 presents two different represen-

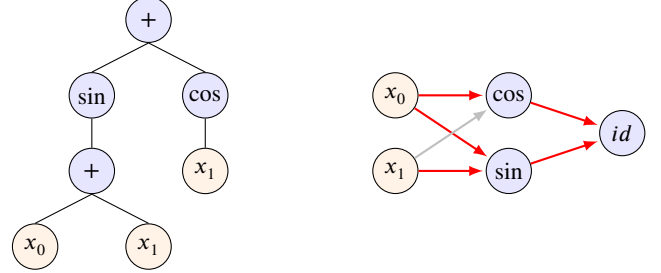


**Figure 14:** Symbolic Tree vs. Symbolic Network.

tations of the equation  $\sin(x_0 + x_1) + \cos(x_1)$ . As shown in the figure, the depth of the symbolic tree is 3, whereas the number of hidden layers in our symbolic network is only 2.

**id Operators:** In symbolic networks, the identity operator  $id$ , which performs an identity transformation, facilitates cross-layer connections for identical modules, thereby eliminating redundant subtrees. In Fig. 15, we use  $g(\cdot)$  to represent the same module. As the complexity of  $g(\cdot)$  increases, the advantage of the  $id$  operator becomes increasingly significant.

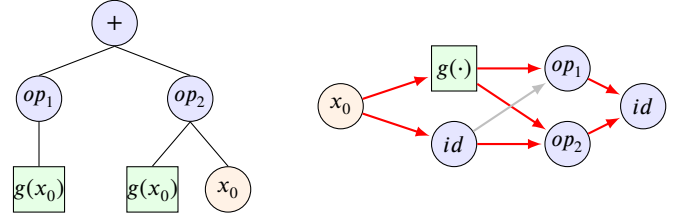


**Figure 15:** Symbolic Tree vs. Unified Symbolic Network.

**Nested Unary Operators:** Symbolic trees and EQL-type symbolic networks typically use standard binary operators. In UniSymNet, we represent binary operators using nested unary operators. The advantages and applicable conditions of this transformation have been discussed in Section 3.1. Of course, this transformation is not entirely beneficial. In some cases, such as for expressions like  $x_1 x_2$ , it may unnecessarily increase the network depth and the number of nodes.

### 6.2. Complexity comparison in a statistical sense

Since the combinations of operators in equations are highly diverse, it is theoretically challenging to compare the complexity of symbolic tree representations and the UniSymNet representations. Therefore, we conduct an empirical comparison of their complexities under controlled conditions.

The structural complexity of both symbolic tree representations and UniSymNet representations can be quantified through two fundamental measures:

- **Depth ( $L$ ):** For symbolic trees, this denotes the longest path from the root node to any leaf node. In UniSymNet, it corresponds to the number of hidden layers.
- **Total number of nodes ( $N$ ):** In symbolic trees, this enumerates all operators and operands within the expression. For UniSymNet, it counts the total nodes across all layers.

The overall complexity is positively correlated with the two measures mentioned above, therefore we define complexity  $C = LN$ . Based on a given frequency distribution of operators, we compare the complexity of the two representations over 100,000 generated expressions. Fig. 16 presents the

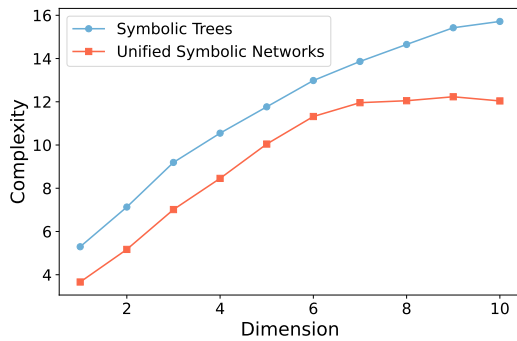


**Figure 16:** Complexity comparison of two representation methods as the dimension varies.

complexity comparison between the two representations. As the dimensionality increases, the complexity gap between UniSymNet and symbolic trees becomes more pronounced, highlighting the advantage of UniSymNet.

## 7. Conclusion

In this work, we propose a novel **Unified Symbolic Network** (UniSymNet), where a pre-trained Transformer model guides structure discovering, and then adopt objective-specific optimization strategies to learn the parameters of the symbolic network. Through experiments on both low-dimensional Standard Benchmarks and high-dimensional SRBench, we demonstrate the outstanding performance of UniSymNet, which not only maintains high fitting accuracy, symbolic solution rate and extrapolation ability, but also ensures a relatively low equation complexity.

## 8. Future works

Future work may focus on two directions: first, improving the label encoding method of UniSymNet to enable end-to-end discovery of mathematical equations from observed data; second, exploring the deployment of UniSymNet in various domains. Specifically, as established in Section 3.1, UniSymNet can achieve lower structural complexity under specific conditions, making it particularly well-suited for applications such as partial differential equation discovery.

## References

- Arnaldo, I., Krawiec, K., O'Reilly, U.M., 2014. Multiple regression genetic programming, in: Proceedings of the 2014 Annual Conference on Genetic and Evolutionary Computation, pp. 879–886.
- Biggio, L., Bendinelli, T., Neitz, A., Lucchi, A., Parascandolo, G., 2021. Neural symbolic regression that scales, in: International Conference on Machine Learning, Pmlr. pp. 936–945.
- Devlin, J., Chang, M.W., Lee, K., Toutanova, K., 2019. Bert: Pre-training of deep bidirectional transformers for language understanding, in: Proceedings of the 2019 conference of the North American chapter of the association for computational linguistics: human language technologies, volume 1 (long and short papers), pp. 4171–4186.
- Dubčáková, R., 2011. Eureka: software review.
- Forrest, S., 1993. Genetic algorithms: principles of natural selection applied to computation. Science 261, 872–878.
- Goodfellow, I., Bengio, Y., Courville, A., Bengio, Y., 2016. Deep learning. volume 1. MIT press Cambridge.
- Hornik, K., Stinchcombe, M., White, H., 1989. Multilayer feedforward networks are universal approximators. Neural networks 2, 359–366.
- Jin, Y., Fu, W., Kang, J., Guo, J., Guo, J., 2019. Bayesian symbolic regression. arXiv preprint arXiv:1910.08892.
- Kamienny, P.A., d'Ascoli, S., Lample, G., Charton, F., 2022. End-to-end symbolic regression with transformers. Advances in Neural Information Processing Systems 35, 10269–10281.
- Keijzer, M., 2003. Improving symbolic regression with interval arithmetic and linear scaling, in: European Conference on Genetic Programming, Springer. pp. 70–82.
- Kim, S., Lu, P.Y., Mukherjee, S., Gilbert, M., Jing, L., Čeperić, V., Soljačić, M., 2020. Integration of neural network-based symbolic regression in deep learning for scientific discovery. IEEE transactions on neural networks and learning systems 32, 4166–4177.
- Kommenda, M., Burlacu, B., Kronberger, G., Affenzeller, M., 2020. Parameter identification for symbolic regression using nonlinear least squares. Genetic Programming and Evolvable Machines 21, 471–501.
- Koza, J.R., 1994. Genetic programming as a means for programming computers by natural selection. Statistics and computing 4, 87–112.
- Krawiec, K., Pawlak, T., 2013. Approximating geometric crossover by semantic backpropagation, in: Proceedings of the 15th annual conference on Genetic and evolutionary computation, pp. 941–948.
- La Cava, W., Orzechowski, P., Burlacu, B., de França, F.O., Virgolin, M., Jin, Y., Kommenda, M., Moore, J.H., 2021. Contemporary symbolic regression methods and their relative performance. arXiv preprint arXiv:2107.14351.
- La Cava, W., Singh, T.R., Taggart, J., Suri, S., Moore, J.H., 2018. Learning concise representations for regression by evolving networks of trees. arXiv preprint arXiv:1807.00981.
- La Cava, W., Spector, L., Danai, K., 2016. Epsilon-lexicase selection for regression, in: Proceedings of the Genetic and Evolutionary Computation Conference 2016, pp. 741–748.
- Lample, G., Charton, F., 2019. Deep learning for symbolic mathematics. arXiv preprint arXiv:1912.01412.
- Lang, S., 2012. Algebra. volume 211. Springer Science & Business Media.
- Li, W., Li, W., Yu, L., Wu, M., Sun, L., Liu, J., Li, Y., Wei, S., Yusong, D., Hao, M., . A neural-guided dynamic symbolic network for exploring mathematical expressions from data, in: Forty-first International Conference on Machine Learning.
- Liu, J., Li, W., Yu, L., Wu, M., Li, W., Li, Y., Hao, M., 2025. Mathematical expression exploration with graph representation and generative graph neural network. Neural Networks , 107405.
- Liu, J., Li, W., Yu, L., Wu, M., Sun, L., Li, W., Li, Y., 2023. Snr: Symbolic network-based rectifiable learning framework for symbolic regression. Neural networks 165, 1021–1034.
- Long, Z., Lu, Y., Dong, B., 2019. Pde-net 2.0: Learning pdes from data with a numeric-symbolic hybrid deep network. Journal of Computational Physics 399, 108925.
- Martius, G.S., Lampert, C., 2017. Extrapolation and learning equations, in: 5th International Conference on Learning Representations, ICLR 2017-Workshop Track Proceedings.

McConaghy, T., 2011. Ffx: Fast, scalable, deterministic symbolic regression technology. *Genetic Programming Theory and Practice IX*, 235–260.

Meurer, A., Smith, C.P., Paprocki, M., Čertík, O., Kirpichev, S.B., Rocklin, M., Kumar, A., Ivanov, S., Moore, J.K., Singh, S., et al., 2017. Sympy: symbolic computing in python. *PeerJ Computer Science* 3, e103.

Mundhenk, T., Landajuela, M., Glatt, R., Santiago, C.P., Petersen, B.K., et al., 2021. Symbolic regression via deep reinforcement learning enhanced genetic programming seeding. *Advances in Neural Information Processing Systems* 34, 24912–24923.

Nocedal, J., Wright, S.J., 1999. *Numerical optimization*. Springer.

Olson, R.S., La Cava, W., Orzechowski, P., Urbanowicz, R.J., Moore, J.H., 2017. Pmlb: a large benchmark suite for machine learning evaluation and comparison. *BioData mining* 10, 1–13.

Petersen, B.K., Larma, M.L., Mundhenk, T.N., Santiago, C.P., Kim, S.K., Kim, J.T., 2020. Deep symbolic regression: Recovering mathematical expressions from data via risk-seeking policy gradients, in: *International Conference on Learning Representations*.

Sahoo, S., Lampert, C., Martius, G., 2018. Learning equations for extrapolation and control, in: *International Conference on Machine Learning*, Pmlr. pp. 4442–4450.

Schmidt, M., Lipson, H., 2009. Distilling free-form natural laws from experimental data. *science* 324, 81–85.

Schmidt, M.D., Lipson, H., 2010. Age-fitness pareto optimization, in: *Proceedings of the 12th annual conference on Genetic and evolutionary computation*, pp. 543–544.

Scholl, P., Bieker, K., Hauger, H., Kutyniok, G., . Parfam–(neural guided) symbolic regression via continuous global optimization, in: *The Thirteenth International Conference on Learning Representations*.

Shojaee, P., Meidani, K., Barati Farimani, A., Reddy, C., 2023. Transformer-based planning for symbolic regression. *Advances in Neural Information Processing Systems* 36, 45907–45919.

de Silva, B.M., Higdon, D.M., Brunton, S.L., Kutz, J.N., 2020. Discovery of physics from data: Universal laws and discrepancies. *Frontiers in artificial intelligence* 3, 25.

Tenachi, W., Ibata, R., Diakogiannis, F.I., 2023. Deep symbolic regression for physics guided by units constraints: toward the automated discovery of physical laws. *The Astrophysical Journal* 959, 99.

Udrescu, S.M., Tegmark, M., 2020. Ai feynman: A physics-inspired method for symbolic regression. *Science Advances* 6, eaay2631.

Uy, N.Q., Hoai, N.X., O’Neill, M., McKay, R.I., Galván-López, E., 2011. Semantically-based crossover in genetic programming: application to real-valued symbolic regression. *Genetic Programming and Evolvable Machines* 12, 91–119.

Valipour, M., You, B., Panju, M., Ghodsi, A., . Symbolicgpt: A generative transformer model for symbolic regression .

Vaswani, A., 2017. Attention is all you need. *Advances in Neural Information Processing Systems* .

Virgolin, M., Alderliesten, T., Bosman, P.A., 2019. Linear scaling with and within semantic backpropagation-based genetic programming for symbolic regression, in: *Proceedings of the genetic and evolutionary computation conference*, pp. 1084–1092.

Virgolin, M., Alderliesten, T., Witteveen, C., Bosman, P.A., 2021. Improving model-based genetic programming for symbolic regression of small expressions. *Evolutionary computation* 29, 211–237.

Wang, Y., Wagner, N., Rondinelli, J.M., 2019. Symbolic regression in materials science. *MRS communications* 9, 793–805.

Wu, M., Li, W., Yu, L., Sun, L., Liu, J., Li, W., 2023. Discovering mathematical expressions through deepsymnet: A classification-based symbolic regression framework. *IEEE Transactions on Neural Networks and Learning Systems* .

## Appendix

### A. Proof of Theorems

In UniSymNet, we transform the nonlinear binary operators  $\{\times, \div, \text{pow}\}$  into nested unary operators through Equation 6. We demonstrate that in Theorem 1, under specific conditions, applying the mapping  $\Psi$  can reduce both the depth and the number of nodes in a symbolic network, thereby lowering its overall complexity. For simplicity, we call the symbolic network with the  $\Psi$  transformation as UniSymNet, and the symbolic network without the  $\Psi$  transformation as EQL-type Network.

First, we introduce a lemma proved an important inequality to be used in the theorem to prepare for the proof of the Theorem 1.

**Lemma 1.** *For integers  $K \geq 2$  and  $d \geq 2$ , the following inequality holds:*

$$K \left( \sum_{i=1}^{\lceil \log_2 d \rceil} \left\lfloor \frac{d}{2^i} \right\rfloor + 1 \right) \geq d + K + 1.$$

PROOF. Let  $S(d) = \sum_{i=1}^{\lceil \log_2 d \rceil} \left\lfloor \frac{d}{2^i} \right\rfloor$ , then:

$$S(d) \geq \sum_{i=1}^{\lceil \log_2 d \rceil} \frac{d}{2^i} = d \cdot \left( 1 - \frac{1}{2^{\lceil \log_2 d \rceil}} \right).$$

Since  $2^{\lceil \log_2 d \rceil} \geq d$ , we have  $\frac{1}{2^{\lceil \log_2 d \rceil}} \leq \frac{1}{d}$ , yielding:

$$S(d) \geq d \left( 1 - \frac{1}{d} \right) = d - 1. \quad (11)$$

Substitute  $S(d) \geq d - 1$  into the left-hand side (LHS) of the original inequality:

$$K \cdot S(d) + 1 \geq K(d - 1) + 1 = Kd - K + 1.$$

To prove  $Kd - K + 1 \geq d + K + 1$ , simplify:

$$Kd - K + 1 - d - K - 1 \geq 0 \quad \Rightarrow \quad d(K - 1) - 2K \geq 0.$$

Rearranging gives:

$$d \geq \frac{2K}{K - 1} = 2 + \frac{2}{K - 1}.$$

Because  $2 < \frac{2K}{K - 1} \leq 4$ , if  $d \geq 4$ , the inequality holds. Then, we just need to verify the condition of  $2 \leq d < 4$ ,  $K \geq 2$ :

- (i)  $d = 2$ :  $S(d) = 2$ ,  $KS(d) = 2K = K + K \geq 2 + K$ ;
- (ii)  $d = 3$ :  $S(d) = 3$ ,  $KS(d) = 3K > 2K \geq 2 + K$ .

Therefore, for all integers  $K \geq 2$  and  $d \geq 2$ , the inequality  $K \left( \sum_{i=1}^{\lceil \log_2 d \rceil} \left\lfloor \frac{d}{2^i} \right\rfloor \right) + 1 \geq d + K + 1$  holds.

Second, we start to prove Theorem 1.

PROOF. Consider  $P(\mathbf{x})$  in  $\mathbb{R}^d$  with  $d \geq 2$ ,

$$P(\mathbf{x}) = \sum_{k=1}^K c_k \prod_{i=1}^d x_i^{m_{ki}}, \quad X = (x_1, \dots, x_d)$$

where  $m_{ki} \in \mathbb{R}$  denotes the exponent of variable  $x_i$  in the  $k$ -th monomial. Applying the unified transformation  $\Psi$  defined in Equation 6, we obtain:

$$\begin{aligned} \Psi(P(\mathbf{x})) &= \Psi \left( \sum_{k=1}^K c_k \prod_{i=1}^d x_i^{m_{ki}} \right) \\ &= \sum_{k=1}^K c_k \exp \left( \sum_{i=1}^d m_{ki} \ln x_i \right) \end{aligned} \quad (12)$$

This transformation enables representation through the following UniSymNet architecture:

- **Layer 1 (ln operators):** Compute  $\{\ln x_i\}_{i=1}^d$  using  $d$  nodes.
- **Layer 2 (exp operators):** Compute  $\exp\left(\sum_{i=1}^d m_{ki} \ln x_i\right)$  using  $K$  nodes.
- **Layer 3 (id operators):** if  $K = 1$ , this layer is not necessary. Otherwise, a id node is needed to apply the linear combination.

Consequently, Any symbolic function  $P(\mathbf{x})$  satisfying the above conditions can be exactly represented by a UniSymNet with depth  $L_1$  and at most  $N_1$  nodes, where

$$\begin{cases} L_1 = 2, N_1 = d + 1, & \text{if } K = 1, \\ L_1 = 3, N_1 = d + K + 1, & \text{else } K \geq 2. \end{cases}$$

If we use normal binary operators in EQL-type networks, the representation of  $P(\mathbf{x})$  through the following architecture:

- **Section 1 ( $(\cdot)^k$  operators):** given the condition:

$$\exists(k_0, i_0), \text{ s.t. } m_{k_0 i_0} \neq 1,$$

at least one additional layer with power-function activations is necessary to construct non-unit exponents. if  $K = 1$ , there are  $d$  nodes in the layer. However, if  $K \geq 2$ , since the depth required for each item may be inconsistent, such as  $x_1 x_2$  and  $x_1^2 x_2$ , exploring the number of nodes is complex. Therefore, if  $K \geq 2$ , we will ignore the number of nodes required for this section.

- **Section 2 ( $\times$  operators):**  $\forall k, \forall i, m_{ki} \neq 0$ , the monomial  $\prod_{i=1}^d x_i^{m_{ki}}$  inherently involves multiplicative interactions across all  $d$  variables. Since the multiplication operator  $\times$  is strictly binary, constructing such a monomial requires a network depth of  $\lceil \log_2 d \rceil$ , with each layer  $i$  containing  $K \lceil \frac{d}{2^i} \rceil$  nodes to iteratively merge pairs of terms.

- **Section 3 (id operators):** if  $K = 1$ , this layer is not necessary. Otherwise, a id node is needed to apply the linear combination.

Consequently, Any symbolic function  $P(\mathbf{x})$  satisfying the above conditions can be exactly represented by a EQL-type network with depth  $L_2$  and at least  $N_2$  nodes, where

$$\begin{cases} L_2 = \lceil \log_2 d \rceil + 1, N_2 = \sum_{i=1}^{\lceil \log_2 d \rceil} \left\lceil \frac{d}{2^i} \right\rceil + d, & \text{if } K = 1, \\ L_2 = \lceil \log_2 d \rceil + 2, N_2 \geq \sum_{i=1}^{\lceil \log_2 d \rceil} \left\lceil \frac{d}{2^i} \right\rceil + 1, & \text{else } K \geq 2. \end{cases}$$

When  $K = 1$ , if  $d \geq 2$ , then  $L_2 = \lceil \log_2 d \rceil + 1 \geq 2 = L_1$ . According to Equation 11, we have  $N_2 \geq d + d - 1 \geq d + 1 = N_1$ ; When  $K \geq 2$ , if  $d \geq 2$ , then  $L_2 = \lceil \log_2 d \rceil + 2 \geq 3 = L_1$ . On the basis of Lemma 1, we have  $N_2 \geq N_1$ . That is to say, when the above conditions are met, when representing the same  $P(\mathbf{x})$ , the depth and the number of nodes of UniSymNet are less than those of EQL.

Finally, we will prove Theorem 2.

PROOF. By replacing  $x_i$  in Theorem 1 with the function  $g_i(x)$ , this is essentially treating it as the first layer input of a neural network.

Let  $P(\mathbf{x})$  require a UniSymNet with depth  $L_{10}$  and node count  $N_{10}$ . Then the total depth is  $L_1 = L_{10} + \max\{L_{1i}\}$ , and the total node count is  $N_1 = N_{10} + \sum_i N_{1i}$ . For the EQL-type symbolic network, let  $P(\mathbf{x})$  require a depth of  $L_{20}$  and a node count of  $N_{20}$ . Then, the total depth is  $L_2 = L_{20} + \max\{L_{2i}\}$ , and the total node count is  $N_2 = N_{20} + \sum_i N_{2i}$ .

Assuming the hypothesis in Theorem 1 holds, then  $L_{10} \leq L_{20}$  and  $N_{10} \leq N_{20}$ . Therefore,

$$\begin{aligned} L_1 &= L_{10} + \max_i \{L_{1i}\} \leq L_{20} + \max_i \{L_{2i}\} = L_2, \\ N_1 &= N_{10} + \sum_i N_{1i} \leq N_{20} + \sum_i N_{2i} = N_2. \end{aligned} \quad (13)$$

## B. Description of the Training Data

In this work, we generated two training sets based on the dimensions ( $d \leq 4$ ) and ( $d > 4$ ). Table 3 provides the specific hyperparameters used for generating these training sets, including details on the range of values for each parameter, the underlying distribution.

## C. Description of the Testing Data

### C.1. Artificial DataSet in Ablation Studies

In the ablation study section, we randomly generated 200 equations with the constraint that the input dimension  $d \leq 4$ ,  $L \leq 6$ . Fig. 17 depict the relationship among the input dimension, label length, and the number of hidden layers within our dataset.

**Table 3**  
Hyperparameters for Data Generation.

| Hyperparameter                     | Symbol           | Value  |  |
|------------------------------------|------------------|--|--|
|                                    |                  | $d \leq 4$   | $d > 4$                                    |
| Max Input Dimension                | $d_{\max}$       | 4  | 10   |
| Max Binary Operators               | $b_{\max}$       | $d + 5$  | $d + 1$                                    |
| Max Hidden Layers                  | $L_{\max}$       | 6  | 7  |
| Number of repetitions of operators | $m$              | 5  | 7  |
| Number of Functions                | -                | 1,500,000  | 3,750,000                                  |
| Input Dimension Distribution       | -                | {1:0.1,2:0.2,3:0.3,4:0.4}  | {5:0.2,6:0.2,7:0.15,8:0.15,9:0.15,10:0.15} |
| Train Data Points                  | $N$              | 200  |  |
| Max Unary Operators                | $u_{\max}$       | $\min\{5, d + 1\}$   |  |
| Binary Operator Sampling Frequency | -                | {add: 1, sub: 1, mul: 1, pow: 1}   |  |
| Unary Operator Sampling Frequency  | -                | {log: 0.3, exp: 1.1, sin: 1.1, cos: 1.1, sqrt: 3, inv: 5, abs: 1, pow2: 2}                                   |  |
| Distribution of $(w, b)$           | $D_{\text{aff}}$ | {sign $\sim \mathcal{U}(-1, 1)$ , {mantissa $\sim \mathcal{U}(0, 1)$ , {exponent $\sim \mathcal{U}(-1, 1)$ } |  |

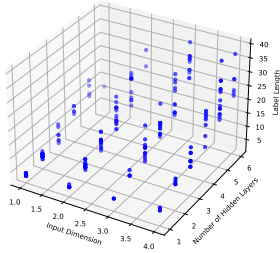


**Figure 17:** 3D scatter plot of artificial dataset.

## C.2. Standard Benchmarks

In the Standard Benchmarks, the equations feature an input dimension  $d \leq 2$  spanning a total of eight datasets. Training sets are generated by sampling points through expressions (detailed in Table 4, with a fixed random seed for consistency). In contrast, testing sets consist of 100 points sampled from the same intervals but with a different random seed, ensuring an independent evaluation of model performance. For a fair comparison, the dataset used in all methods was generated under the same seed.

## C.3. SRBench

In SRBench, most equations have an input dimension  $2 \leq d \leq 10$ , covering two datasets in total: Feynman and Strogatz. The Feynman dataset comprises a total of 119 equations sourced from Feynman Lectures (Udrescu and Tegmark, 2020) on Physics database series. The Strogatz dataset contains 14 SR problems sourced from the ODE-Strogatz database.

## D. Computing Infrastructure

The experiments in this work were executed on an Intel(R) Xeon(R) Gold 6330 CPU @ 2.00GHz, 1.5T RAM equipped with two NVIDIA A100 GPUs 80GB.

**Table 4**  
Standard Benchmarks: Part 1.

| Name       | Expression                        |
|------------|-----------------------------------|
| Nguyen-1   | $x^3 + x^2 + x$                   |
| Nguyen-2   | $x^4 + x^3 + x^2 + x$             |
| Nguyen-3   | $x^5 + x^4 + x^3 + x^2 + x$       |
| Nguyen-4   | $x^6 + x^5 + x^4 + x^3 + x^2 + x$ |
| Nguyen-5   | $\sin(x^2) \cos(x) - 1$           |
| Nguyen-6   | $\sin(x) + \sin(x + x^2)$         |
| Nguyen-7   | $\log(x + 1) + \log(x^2 + 1)$     |
| Nguyen-8   | $\sqrt{x}$                        |
| Nguyen-9   | $\sin(x) + \sin(y)$               |
| Nguyen-10  | $2 \sin(x) \cos(y)$               |
| Nguyen-11  | $x^y$                             |
| Nguyen-12  | $x^4 - x^3 + \frac{1}{2}y^2 - y$  |
| Nguyen-1c  | $3.39x^3 + 2.12x^2 + 1.78x$       |
| Nguyen-5c  | $\sin(x^2) \cos(x) - 0.75$        |
| Nguyen-7c  | $\log(x + 1.4) + \log(x^2 + 1.3)$ |
| Nguyen-8c  | $\sqrt{1.23x}$                    |
| Nguyen-10c | $\sin(1.5x) \cos(0.5y)$           |
| Constant-1 | $3.39x^3 + 2.12x^2 + 1.78x$       |
| Constant-2 | $\sin(x^2) \cos(x) - 0.75$        |
| Constant-3 | $\sin(1.5x) \cos(0.5y)$           |
| Constant-4 | $2.7xy$                           |
| Constant-5 | $\sqrt{1.23x}$                    |
| Constant-6 | $x^{0.426}$                       |
| Constant-7 | $2 \sin(1.3x) \cos(y)$            |
| Constant-8 | $\log(x + 1.4) + \log(x^2 + 1.3)$ |
| R-1        | $\frac{(x+1)^3}{x^2-x+1}$         |
| R-2        | $\frac{x^2-3x^3+1}{x^2+x^5}$      |
| R-3        | $\frac{x^0+x^5}{x^4+x^3+x^2+x+1}$ |
| Koza-2     | $x^5 - 2x^3 + x$                  |
| Koza-4     | $x^6 - 2x^4 + x^2$                |

**Table 4**  
Standard Benchmark: Part 2

| Name         | Expression   |
|--------------|--|
| Livermore-1  | $\frac{1}{3} + x + \sin(x^2)$                          |
| Livermore-2  | $\sin(x^2) \cos(x) - 2$                                |
| Livermore-3  | $\sin(x^3) \cos(x^2) - 1$                              |
| Livermore-4  | $\log(x + 1) + \log(x^2 + 1) + \log(x)$                |
| Livermore-5  | $x^4 - x^3 + x^2 - x$                                  |
| Livermore-6  | $4x^4 + 3x^3 + 2x^2 + x$                               |
| Livermore-7  | $\sinh(x)$   |
| Livermore-8  | $\cosh(x)$   |
| Livermore-9  | $x^9 + x^8 + x^7 + x^6 + x^5 + x^4 + x^3 + x^2 + x$    |
| Livermore-10 | $6 \sin(x) \cos(y)$                                    |
| Livermore-11 | $\frac{x^2+y^2}{x+y}$                                  |
| Livermore-12 | $\frac{x^4}{y^4}$                                      |
| Livermore-13 | $x^{\frac{2}{3}}$                                      |
| Livermore-14 | $x^3 + x^2 + x + \sin(x) + \sin(x^2)$                  |
| Livermore-15 | $x^{\frac{1}{5}}$                                      |
| Livermore-16 | $x^{\frac{2}{5}}$                                      |
| Livermore-17 | $4 \sin(x) \cos(y)$                                    |
| Livermore-18 | $\sin(x^2) \cos(x) - 5$                                |
| Livermore-19 | $x^5 + x^4 + x^2 + x$                                  |
| Livermore-20 | $\exp(-x^2)$   |
| Livermore-21 | $x^8 + x^7 + x^6 + x^5 + x^4 + x^3 + x^2 + x$          |
| Livermore-22 | $\exp(-0.5x^2)$  |
| Keijzer-3    | $0.3 \cdot x \cdot \sin(2\pi x)$                       |
| Keijzer-4    | $x^3 \exp(-x) \cos(x) \sin(x) (\sin(x^2) \cos(x) - 1)$ |
| Keijzer-6    | $\frac{x(x+1)}{2}$                                     |
| Keijzer-7    | $\ln x$  |
| Keijzer-8    | $\sqrt{x}$   |
| Keijzer-9    | $\log(x + \sqrt{x^2 + 1})$                             |
| Keijzer-10   | $x^y$  |
| Keijzer-11   | $xy + \sin((x-1)(y-1))$                                |
| Keijzer-12   | $x^4 - x^3 + \frac{y^2}{2} - y$                        |
| Keijzer-13   | $6 \sin(x) \cos(y)$                                    |
| Keijzer-14   | $\frac{8}{2+x^2+y^2}$                                  |
| Keijzer-15   | $\frac{x^3}{5} + \frac{y^3}{2} - y - x$                |
| Jin-1        | $2.5x^4 - 1.3x^3 + 0.5y^2 - 1.7y$                      |
| Jin-2        | $8.0x^2 + 8.0y^3 - 15.0$                               |
| Jin-3        | $0.2x^3 + 0.5y^3 - 1.2y - 0.5x$                        |
| Jin-4        | $1.5 \exp(x) + 5.0 \cos(y)$                            |
| Jin-5        | $6.0 \sin(x) \cos(y)$                                  |
| Jin-6        | $1.35xy + 5.5 \sin((x-1.0)(y-1.0))$                    |

## E. Hyperparameter Settings

The hyperparameters involved in the experiment are shown in Table 5. It is important to note that some parameters may change depending on the specific problem. For instance, the training epochs in Network Training will vary with the number of hidden layers  $L$ .

## F. Algorithms for Label Encoding

To implement label encoding, it is crucial to convert function expressions in string form into a network structure. For this purpose, we employ the following Algorithm 2.

**Table 5**  
Hyperparameters for UniSymNet.

| Hyperparameter                          | Symbol         | Value                     |
|---|----------------|---------------------------|
| <b>Pre-Training</b>                     |                |                           |
| Learning rate                           | $\eta$         | 0.0001                    |
| Learning rate decay                     | $\gamma$       | 0.99                      |
| Batch size                              | $B$            | 512                       |
| Embedding size                          | -              | 512                       |
| Training epochs                         | $K$            | $20(d \leq 4), 40(d > 4)$ |
| <b>Beam Search</b>                      |                |                           |
| Beam size                               | -              | 20                        |
| Number of candidate structure sequences | -              | 5                         |
| <b>Network Training</b>                 |                |                           |
| Learning rate                           | $\eta$         | 0.01                      |
| Batch size                              | $B$            | 64                        |
| Weight initialization parameter         | -              | 2                         |
| Training epochs                         | $K$            | 10L                       |
| Penalty threshold of $\log_{reg}$       | $\theta_{log}$ | 0.0001                    |
| Penalty threshold of $\exp_{reg}$       | $\theta_{exp}$ | 100                       |
| Penalty Epoch                           | -              | 10                        |
| <b>BFGS</b>                             |                |                           |
| Number of restarts                      | -              | 10                        |
| Number of points                        | -              | 200                       |
| Random exponent                         | -              | {-1, -2, 1, 2, 3, 0.5}    |

**Algorithm 2** Structure Identification for UniSymNet

- 1: **Input:** Symbolic expression  $expr$ , dimension  $d$
- 2: Initialize UniSymNet’s structure list  $\mathcal{L}$
- 3:  $\mathcal{L} \leftarrow [[id]]$
- 4:  $(L_{op}, L_{expr}) \leftarrow \text{SYMBOLICDECOMPOSE}(expr)$
- 5:  $\mathcal{L} \leftarrow \mathcal{L} \circ L_{op}$
- 6: **while**  $L_{op} \neq \emptyset$  **do**
- 7:    $\mathcal{T}_{op} \leftarrow \emptyset, \mathcal{T}_{expr} \leftarrow \emptyset$
- 8:   **for**  $\sigma \in L_{expr}$  **do**
- 9:     **if**  $\sigma$  is nested **then**
- 10:        $\{(\tau_{op}^{(i)}, \tau_{expr}^{(i)})\}_{i=1}^k \leftarrow \text{RECURSIVEPARSE}(\sigma)$
- 11:        $\mathcal{T}_{op} \leftarrow \mathcal{T}_{op} \cup \{\tau_{op}^{(i)}\}, \mathcal{T}_{expr} \leftarrow \mathcal{T}_{expr} \cup \{\tau_{expr}^{(i)}\}$
- 12:     **else**
- 13:        $(\tau_{op}, \tau_{expr}) \leftarrow \text{SYMBOLICDECOMPOSE}(\sigma)$
- 14:        $\mathcal{T}_{op} \leftarrow \mathcal{T}_{op} \cup \{\tau_{op}\}, \mathcal{T}_{expr} \leftarrow \mathcal{T}_{expr} \cup \{\tau_{expr}\}$
- 15:     **end if**
- 16:   **end for**
- 17:    $\mathcal{L} \leftarrow \mathcal{L} \circ \mathcal{T}_{op}$
- 18:    $L_{op} \leftarrow \text{FLATTEN}(\mathcal{T}_{op}), L_{expr} \leftarrow \text{FLATTEN}(\mathcal{T}_{expr})$
- 19: **end while**
- 20:  $\mathcal{L} \leftarrow \text{PRUNE}(\mathcal{L})$
- 21: **Output:**  $\mathcal{L}$

## G. Comprehensive Overview of Baselines

### G.1. In-domain Methods

Our in-domain methods include six approaches, with EQL and DySymNet being a learning-from-scratch method, while the remaining four are learning-with-experience methods. Table 6 provides a detailed description of the in-domain methods.

**Table 6**  
Comprehensive Overview of In-domain Baselines.

| Method     | Description  |
|------------|--|
| EQL        | A method(Sahoo et al., 2018) that directly trained a fully connected neural network without any guidance on changing the symbolic network framework.   |
| DySymNet   | A RL-based method(Li et al.) uses a controller for sampling various architectures of symbolic network guided by policy gradients.  |
| ParFam     | A novel algorithm(Scholl et al.) that leverages the inherent structural patterns of physical formulas to transform the original discrete optimization problem into a continuous one, making the search process more efficient and tractable. |
| NeSymRes   | A Transformer-based method(Biggio et al., 2021) that used a pre-trained model to obtain the equation’s skeleton, treating operators (e.g., '+', '-', 'exp', 'log') as tokens.  |
| End-to-end | A Transformer-based method(Kamienny et al., 2022) that didn’t rely on skeleton structures, using a hybrid symbolic-numeric vocabulary that encoded both symbolic operators and variables, as well as numeric constants.                      |
| TPSR       | A Transformer-based method(Shojaee et al., 2023) for Symbolic Regression that incorporates Monte Carlo Tree Search planning algorithm into the transformer decoding process.   |

## G.2. Out-of-domain Methods

We present concise descriptions of the 14 SR baseline methodologies employed by SRBench, as depicted in Table 7. These 14 methods include both GP-based and deep learning-based approaches.

**Table 7**  
Comprehensive Overview of Out-of-domain Baselines.

| Method      | Description   |
|-------------|---|
| BSR         | A method (Jin et al., 2019) generates models as a linear combination of symbolic trees using a Markov Chain Monte Carlo algorithm.  |
| AlFeynman   | A divide-and-conquer method (Udrescu and Tegmark, 2020) uses neural networks to identify modularities and decompose problems into simpler subproblems.  |
| AFP         | A method (Schmidt and Lipson, 2010) incorporates model age as an objective to prevent premature convergence and bloat.  |
| AFP_FE      | A method combines AFP with Eureqa’s method for fitness estimation.  |
| EPLEX       | A parent selection method (La Cava et al., 2016) filters models through randomized subsets of training cases, rewarding those that excel in challenging data regions.                                   |
| FEAT        | A method (La Cava et al., 2018) focuses on discovering simple solutions that generalize well by storing solutions with accuracy-complexity trade-offs.  |
| FFX         | A method (McConaghy, 2011) initializes a population of equations, selects the Pareto optimal set, and returns a single linear model by treating the population as features.                             |
| GP(gplearn) | A method initializes a random population of models and iteratively applies selection, mutation, and crossover operations.   |
| GP-GOMEA    | A method(Virgolin et al., 2021) that adapts recombination by modeling interdependencies and recombining components to preserve collaboration.   |
| DSR         | A method (Petersen et al., 2020) uses RL to train a generative RNN model of symbolic expressions, employing a risk-seeking policy gradient to bias the model towards exact expressions.                 |
| ITEA        | A method (de Silva et al., 2020) where each model is an affine combination of interaction-transformation expressions, comprising a unary transformation function and a polynomial interaction function. |
| MRGP        | A method(Arnaldo et al., 2014) where the entire program trace, including each sub-function of the model, is decomposed into features and used to train a Lasso model.                                   |
| Operon      | A method (Kommenda et al., 2020) integrates non-linear least squares constant optimization through the Levenberg-Marquardt algorithm within a GP framework.   |
| SBP-GP      | A method (Virgolin et al., 2019) refines SBP-based recombination by dynamically adjusting outputs via affine transformations.   |